Distributed Beams: Concept of Operations for Polarimetric Rotating Phased Array Radar

David Schvartzman, *Member, IEEE*, Sebastián M. Torres, *Senior Member, IEEE*, and Tian-You Yu, *Member, IEEE*

***Abstract*— Important requirements for a future generation of weather surveillance radars include improvements in data quality and more rapid update of volumetric data. Phased array radar (PAR) is a candidate technology capable of providing the required functionality. The rotating PAR (RPAR) is a potential architecture that could improve the capabilities of the current parabolic-reflector-based US Weather Surveillance Radar—1988 Doppler (WSR-88D) operational network and is more affordable than other candidate PAR architectures. However, RPAR concept of operations that support observational needs has to be developed. The *Distributed Beams* (DB) technique introduced in this article provides a way to either reduce the scan times or to reduce the variance of radar-variable estimates by azimuthally spoiling the transmit beam while receiving multiple digital beams as the radar rotates in azimuth. Specifically, the rotation speed of the pedestal is derived from the duration of the coherent processing interval (CPI) to produce the desired spatial sampling. This results in beams from subsequent CPIs in approximately the same directions, which increases the number of available data samples for processing. The increased number of available samples can be coherently processed to reduce the variance of estimates. Alternatively, by reducing the number of samples per CPI and increasing the RPAR's rotation rate, the scan time can be reduced without increasing the variance of estimates. Results presented demonstrate both applications of the DB technique for dual-polarization observations. Given that this technique makes use of spoiled transmit beams, its benefits come at the expense of degraded angular resolution (beamwidth and sidelobe levels), and reduced sensitivity compared with the use of pencil beams. The technique could be implemented as part of an RPAR concept of operations to meet requirements for the future weather surveillance network if certain tradeoffs are accounted for in the radar design process.**

Manuscript received June 17, 2020; revised August 14, 2020 and November 25, 2020; accepted December 20, 2020. Funding was provided by National Oceanic and Atmospheric Administration (NOAA)/Office of Oceanic and Atmospheric Research under NOAA-University of Oklahoma Cooperative Agreement #NA16OAR4320115, U.S. Department of Commerce. *(Corresponding author: David Schvartzman.)*

David Schvartzman and Sebastián M. Torres are with the Cooperative Institute for Mesoscale Meteorological Studies, The University of Oklahoma, Norman, OK 73069 USA, also with the NOAA/OAR/National Severe Storms Laboratory, Norman, OK 73072 USA, and also with the Advanced Radar Research Center, School of Electrical and Computer Engineering, University of Oklahoma, Norman, OK 73069 USA (e-mail: david.schvartzman@noaa.gov).

Tian-You Yu is with the Advanced Radar Research Center, School of Electrical and Computer Engineering, University of Oklahoma, Norman, OK 73069 USA, and also with the School of Meteorology, The University of Oklahoma, Norman, OK 73069 USA.

Color versions of one or more figures in this article are available at https://doi.org/10.1109/TGRS.2020.3047090.

Digital Object Identifier 10.1109/TGRS.2020.3047090

***Index Terms*— phased array radar, rotating phased array radar, digital beamforming, weather radar, dual-polarization, concept of operations.**

I. Introduction

THE National Oceanic and Atmospheric Administration (NOAA) has started considering radar systems for the eventual replacement of the operational U.S. Weather Surveillance Radar – 1988 Doppler (WSR-88D), which is projected to reach the end of its operational lifetime by 2040 [1]. In addition to the current operational capabilities of the WSR-88D to detect, estimate, and classify returns from meteorological scatterers with high sensitivity and spatial resolution, NOAA has defined performance requirements that involve a more rapid update of volumetric data, and the ability to perform adaptive weather observations [2]. This network of 160 Doppler weather radars was upgraded in 2012 to simultaneously transmit and receive electromagnetic waves in both horizontal and vertical polarizations, which provided these radars with dual-polarization capability [3]. The received signals on the horizontal (H) and vertical (V) polarization channels are used to estimate conventional spectral moments (reflectivity, Doppler velocity, and spectrum width, which are computed using data from the H-polarization channel) and polarimetric variables (differential reflectivity, differential phase, and co-polar correlation coefficient, which are computed using data from both the H- and V-polarization channels). This enables the classification of meteorological scatterers (e.g., rain, graupel, large hail, snow) and non-meteorological targets (e.g., insects, birds, and chaff), which supports the downstream improvement of algorithms such as quantitative precipitation products [4], [5]. Polarimetric variables have become a fundamental tool for better interpretation and forecasting of hazardous weather events, and maintaining or improving the quality of estimates is critical to support the National Weather Service (NWS) mission [6]. Nevertheless, intrinsic architecture limitations may prevent parabolic-reflector systems (such as the WSR-88D) from attaining the performance levels required to meet the set of next-generation radar functional requirements specified by the NOAA.

The NOAA Radar Functional Requirements document [2] specifies the functionality expected for a future weather surveillance radar system. The document's *Threshold Functional Requirements* are used to define the minimum expected performance of the future system, while its *Optimal Functional*

Requirements define the desired system performance. One of the most demanding optimal requirements is the 1-minute update time to complete a volume scan "*with no degradation of the sensitivity, spatial resolution or standard deviation (SD) of measurement for radar variable estimates*." To achieve this volume-update-time requirement with quality radar-variable estimates, advanced scanning and digital signal processing techniques are needed.

Unique and flexible capabilities offered by phased array radar (PAR) technology support the required enhanced weather surveillance strategies that are envisioned to improve the weather radar products, making PAR technology an attractive candidate for the next generation of weather radars. Important research efforts documented in [7] and [8] illustrate the advantages of PAR technology over conventional reflector-antenna radars for weather observations and motivate further studies. Ongoing research efforts that began in the early 2000s at the National Severe Storms Laboratory (NSSL) have aimed at demonstrating unique PAR capabilities for weather surveillance [9], [10]. The phased array radar innovative sensing experiment (PARISE [11]) was designed to demonstrate the advantages of rapid-scan PAR data to improve the ability of forecasters to warn of severe weather [12]. Researchers have also reported that PAR rapid scan data are expected to enhance the effectiveness of radar data assimilation and numerical weather prediction systems [13].

From these previous studies, a stationary four-faced planar PAR architecture has been the prime candidate system involving a multifunction phased array radar (MPAR) system that would simultaneously support several missions [14]. Nevertheless, the discrepancies among interagency deployment timelines (aided by the insufficient maturity of polarimetric PAR technology for weather observations) resulted in the MPAR concept becoming a less feasible option. Consequently, current efforts are now centered on single-mission systems. While a four-faced PAR is expected to achieve the optimal requirements set forth by NOAA, deploying and maintaining an operational network of these radars across the U.S. may be unaffordable. A more affordable alternative radar system is based on a single-faced rotating PAR (RPAR) architecture [15], which is capable of meeting the threshold requirements and exceeding the capabilities of the current reflector-based WSR-88D network. However, to achieve current and future needs to support the NWS mission, advanced concept of operations (CONOPS) for weather surveillance using the RPAR has to be developed.

The RPAR architecture has been used for air surveillance and defense applications since the late 1970s [16]–[18] but was only introduced for weather surveillance in recent years [19]–[23]. The CONOPS for these weather RPAR systems consist of either imitating the operation of conventional reflector radar with continued mechanical rotation and performing a straightforward electronic scan in elevation, or exploiting radar imaging (i.e., transmitting a wide beam) and digital beamforming in elevation while rotating in azimuth. While some of these operational concepts make use of RPAR's unique capabilities in support of meeting functional requirements, alternative concepts and their associated tradeoffs should be explored. Important tradeoffs will have to be considered for designing the RPAR CONOPS, and several scanning techniques operating in conjunction may be needed to meet demanding requirements.

The purpose of this article is to introduce the distributed beams (DB) technique which provides a way to reduce scan update times or to improve the data quality for a dual-polarization RPAR CONOPS. Digital beamforming in elevation has been demonstrated to reduce the scan time for single-polarization weather RPARs [20], [22]. While it has been proposed in azimuth [24], the novelty of the technique introduced in this work is in the coherent processing of samples from subsequent receive beams. This is accomplished by synthesizing an azimuthally wide (*spoiled*) beam on transmission and then using digital beamforming to form several simultaneous beams on reception as the radar rotates (herein referred to as a cluster of receive beams). Examples of transmit beam patterns with spoil factors (F) of 3 and 5, as well as the inherent narrow beam pattern for the array synthesizing them are presented in Fig. 1. Specifically, the azimuthal rotation rate of the platform is derived from the duration of the coherent processing interval (CPI), to produce the desired spatial sampling. Consequently, beams from subsequent CPIs are received from approximately the same direction. For example, if the antenna rotates in the clockwise direction and the receive beams in a cluster are numbered in the same direction, both the last receive beam from the first cluster and the second-to-last receive beam from the second cluster point at the same azimuth. An illustration of this concept is presented in Fig. 2. This increases the number of samples received by a factor equal to the number of beams received in the cluster (herein referred to as R_F). The increased number of available data samples can be processed coherently to reduce the variance of estimates. Alternatively, by reducing the number of samples per CPI and increasing the RPAR's rotation rate (both by R_F), the scan time can be reduced by R_F without increasing the variance of estimates. In summary, the DB technique capitalizes the RPAR mechanical rotation and exploits the use of digital beamforming in azimuth. It allows a faster rotation speed to be maintained, leading to more rapid updates potentially without degradation in data quality. Alternatively, if the rotation speed is maintained, the number of samples can be increased by a factor of R_F, which leads to reduced variance of radar-variable estimates [25]. The DB technique introduced in this article was implemented on NSSL's recently deployed advanced technology demonstrator (ATD) PAR system and it is the first practical demonstration of digital beamforming in azimuth for dual-polarization weather RPAR.

Compared with the use of narrow pencil beams, the use of this technique will result in increased beamwidth, increased sidelobe levels, and reduced sensitivity. That is, an RPAR design to meet spatial resolution and sensitivity requirements [2] using narrow pencil beams may fail to do so when using the proposed technique. In general, the design of a radar antenna that meets specific functional requirements cannot

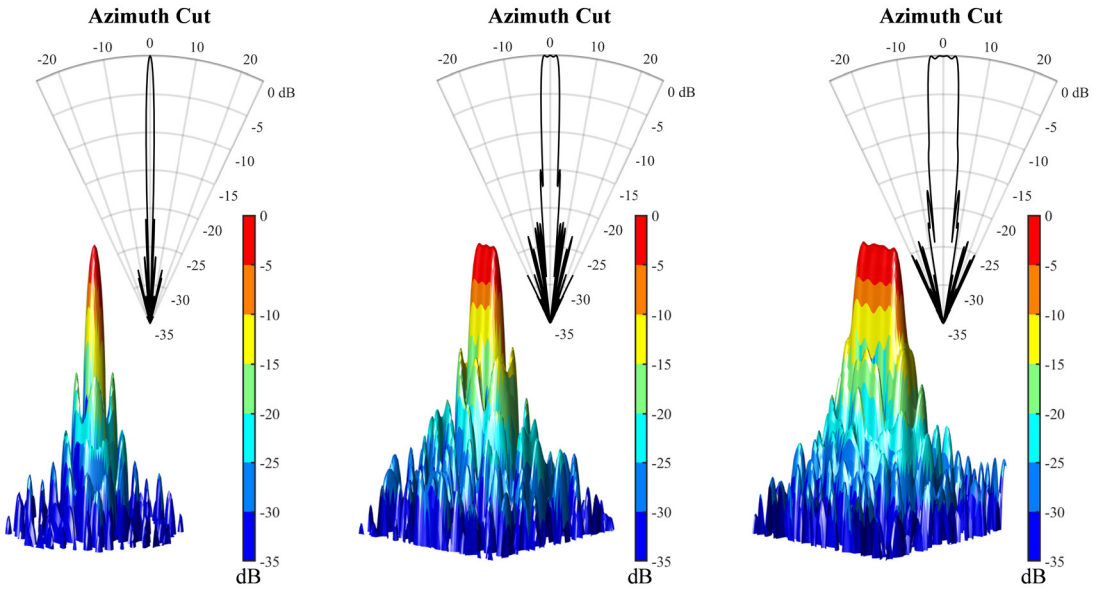

Fig. 1. Simulated one-way antenna radiation patterns for a narrow pencil beam (left), a beam spoiled by a factor of three (center), and a beam spoiled by a factor of five (right). Sectors correspond to azimuthal cuts of the antenna patterns.

be decoupled from its concept of operations. The use of the proposed technique should be considered in the design stages of an RPAR to properly account for the degradation in spatial resolution and sensitivity. Otherwise, an operational mode whereby the DB technique is used to reduce the scan time or the variance of radar-variable estimates can be defined, with the consideration that spatial resolution and/or sensitivity requirements may not be met when using this mode. This could be an acceptable solution if the operational benefits of using the DB technique outweigh any negative data-quality impacts.

The rest of this article is structured into five sections as follows. Section II provides a more detailed technical description of the DB CONOPS and illustrates the two previously discussed applications. Section III then describes the practical implementation of DB, including calibration methods and important considerations for a successful operation. Section IV takes the theoretical analysis further using the experimental implementation for a comparative demonstration of the DB CONOPS by presenting polarimetric weather observations for both applications of the technique. Section V provides the analysis and verification of the radar-variable estimates produced using DB by comparing the data quality to those obtained from data that was collected simultaneously using NSSL's collocated experimental WSR-88D (KOUN) radar system. Section VI summarizes the contributions of this article and discusses alternative RPAR CONOPS using the DB technique.

II. Distributed Beams Technique

Active PAR technology allows the synthesis of antenna radiation beam patterns on transmission by varying the magnitude and phase of transmit signals at each individual array element (commonly referred to as tapering). This capability can be used to produce a wider transmit beam, effectively increasing the beam coverage. This comes at the expense of increased antenna pattern sidelobe levels, reduced antenna gain, and slightly increased beamwidth [26]. For example, an active PAR antenna with an inherent non-tapered radiation pattern that produces a narrow "pencil" beam (as defined by its one-way 3 dB width) can also be used to synthesize wider transmit beams as illustrated in Fig. 1.

Modern PAR can form multiple beams received within a wide transmit beam through digital multichannel receivers [27]. The digitally generated beams are received with the full antenna aperture to produce narrow pencil beams. However, the sidelobe levels of synthesized two-way beams are typically considerably higher, and the beamwidth is slightly increased compared with two-way patterns obtained when using pencil beams on both transmission and reception. This is due to the use of digital beamforming methods, as noted by [20], and the use of a wide spoiled transmit beam, as noted by [28]. For this study, the standard Fourier beamforming method is used to form the receive beams. Considering that digital beamforming is used to form beams within the relatively narrow spoiled beam tapers (worst case for spoiled beams in this article is $\sim\pm 3.2^\circ$ about the broadside) and that the spoiled transmit beams are always on broadside, the increase in sidelobe levels is largely controlled by the spoiled transmit beam pattern.

Researchers demonstrated the use of wide transmit beams and digital beamforming in elevation to reduce the volume scan time of an RPAR [19], [22]. Since operational weather radars typically scan by rotating in the azimuth plane and acquisition parameters such as the PRT are naturally defined as a function of elevation, an advantage for spoiling the beam in azimuth is that operational scan strategies used by radars with rotating reflector antennas can be replicated in an RPAR system. That is, by scanning in azimuth only, identical acquisition parameters (M and T_s) as those in operational scan strategies can be used. When spoiling the beam and scanning in elevation, the same acquisition parameters must be used for

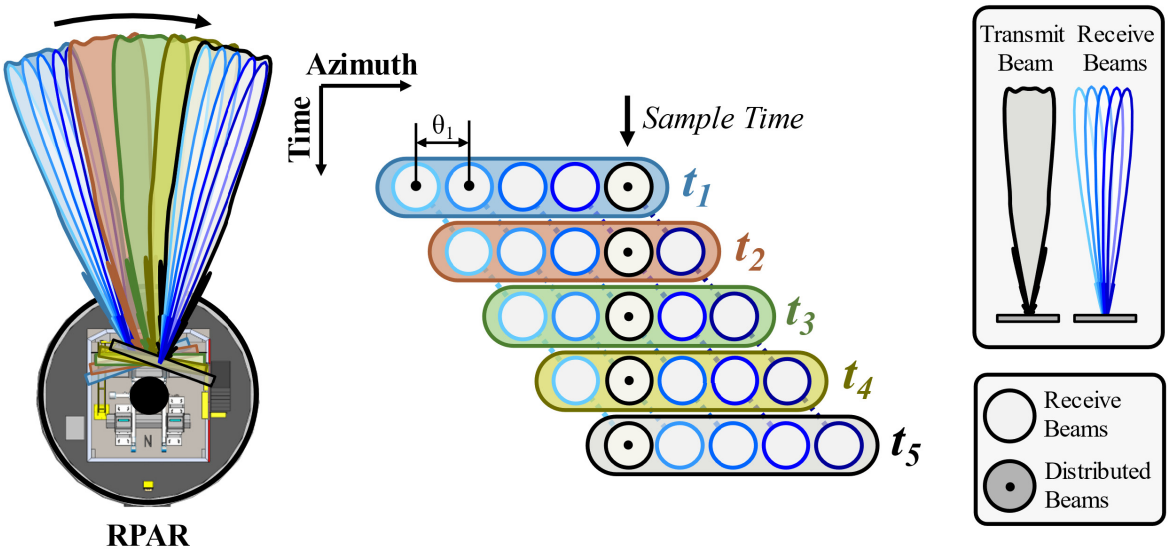

Fig. 2. Illustration of the DBs technique. (Left) Top view of an RPAR system illustrates the radiation of wide transmission beams for which multiple simultaneous beams are received (note that the beams are not drawn to scale). (Center) Diagram shows how receive beams from subsequent transmissions can be grouped to increase the number of samples in a CPI. (Right) Reference for the spoiled transmit beams and the digitally receive beams is shown.

all elevations in the cluster. And while the lower elevations in the WSR-88Ds use two scans of the same elevation (with different PRTs) to mitigate range and velocity ambiguities, higher ones do not. Therefore, spoiling a wide fan beam in elevation could impact the quality of estimates at higher tilts or unnecessarily add more time to the scan. For example, surveillance scans at lower elevation angles use longer PRTs; therefore, using this PRT for scans at higher elevation angles could limit the Nyquist interval (alternatively, the maximum unambiguous range could be impacted if a shorter PRT is used for several scans in elevation). Furthermore, for typical WSR-88D scan strategies, elevation angles scanned at higher altitudes are spread by several degrees. The larger the spoiling factor, the larger the sensitivity loss incurred and the larger the increase in sidelobe levels. Spoiling the beam across angles that are not needed nor typically scanned (i.e., leaving large gaps) will result in an unnecessarily large sensitivity loss. The DB technique could help in these situations by fully utilizing the energy transmitted when spoiling in azimuth.

A CONOPS for the RPAR using the DB technique is now defined. Assume the antenna is rotating in azimuth at a constant speed of ω °s^{-1}, a broadside transmit beam is spoiled by a factor F, and R_F beams are simultaneously generated with digital beamforming techniques within the transmit beam after reception [20]. Typically, the azimuthal sampling for weather surveillance is set to either one beamwidth (θ_1) as illustrated in Fig. 2 (for a factor $F = 5$, and $R_F = 5$) or one-half beamwidth ($0.5\theta_1$, for a factor $F = 5$, and $R_F = 9$). Herein, the sampling spacing of receive beams will be referred to as $\Delta\theta_1$, where Δ is either 1 or 0.5. The one-way half-power beamwidth is defined as the angular width in degrees within which the microwave radiation power is at least one-half of its peak intensity [29]. The two-way beamwidth, which includes the effects of transmit and receive patterns, is defined as the angular width in degrees within which the microwave radiation is at least one-quarter of its peak intensity. Herein, the two-way beamwidth definition is adopted and simply referred to as the beamwidth. Finally, let us assume that the data quality requirement sought in terms of bias and SD of the radar-variables estimates defines the optimal CPI as a set of M pulses at a pulse repetition time (PRT) of T_s seconds. With this, the optimal radar rotation speed ω can be set to,

$$\omega = \frac{\Delta\theta_1}{MT_s}^{\circ} \text{ s}^{-1} \tag{1}$$

in order to collect the desired CPI (MT_s) over the specified angular sampling of $\Delta\theta_1$. It is noted that due to continuous antenna rotation coupled with the need to perform coherent processing of multiple samples, the resulting effective antenna beamwidth is broader than the stationary inherent antenna beamwidth. This effect, referred to as *beam smearing* and defined as the fractional beamwidth increase due to antenna motion and sampling, has been quantified by [30]. As demonstrated in this reference, beam smearing effects are not controlled only by the rotation speed, but rather by the normalized azimuthal sampling spacing, Δ. The value of Δ for all cases illustrated in this article is 0.5, the same as that used in the WSR-88D super-resolution scans. That is, if the CPI is designed using (1) and with Δ of 0.5 or 1, beam smearing effects incurred with the DB technique are analogous to those incurred by the WSR-88D. As mentioned before, there are two applications being considered for the DB CONOPS: 1) scan time reduction and 2) variance reduction.

A. Scan Time Reduction

Applying the DB scan-time reduction strategy requires an increase in the rotation speed. This allows the number of samples per CPI to be reduced to $M_{\text{DB}} = M/R_F$, and the rotation speed to be increased by a factor of R_F to $\omega_{\text{DB}} = R_F\omega$. As the RPAR rotates at ω_{DB}, a pulse train defined by the CPI is continuously transmitted every T_s seconds,

and M_{DB} samples are received per CPI on each digitally generated receive beam. Given that the antenna rotates at $\omega_{\mathrm{DB}} M_{\mathrm{DB}} T_s = \Delta\theta_1$ degrees per CPI and the azimuthal sampling of the R_F receive beams is set to $\Delta\theta_1$, subsequent receive beams (as illustrated in Fig. 2) sample approximately the same azimuth location. That is, in a continuous rotation regime, ω_{DB} is such that the centers of resolution volumes (defined by the effective beamwidths in azimuth and elevation, and the range resolution) sampled by the set of R_F beams received every $M_{\mathrm{DB}} T_s$ seconds (from distinct transmit beams) are associated with approximately the same location in space. Samples received on these different transmit–receive beams can then be coherently processed to get the $M_{\mathrm{DB}} R_F = M$ samples required to obtain the desired data quality. Operating the radar under this DB CONOPS results in reducing the scan time by a factor R_F while maintaining the same variance of radar-variable estimates.

Comparing this DB CONOPS to that from a conventional radar with a parabolic-reflector antenna, the DB technique exploits the RPAR beamforming capability to reduce the scan time. This comes at the expense of: 1) increased rotation speed; 2) two-way pattern increased sidelobe levels [28]; 3) reduced sensitivity; and 4) an increased two-way beamwidth due to the wider transmit beam. However, it is believed that some of the listed limitations can be mitigated. The rotation speed increase is technically possible as argued by [31], since the rotating machinery is a mature technology and has a high technology-readiness level. This reduces the risk of deploying and maintaining RPAR pedestals capable of rotating at higher speeds. The beamwidth and sidelobe level increases of the two-way pattern could be reduced to the desired levels by increasing the aperture size. This would entail the use of a more aggressive taper on the receiving array to lower sidelobe levels [32] and such that the resulting two-way beamwidth and sidelobe levels meet the desired requirements [2]. The amount by which the aperture has to be increased to achieve similar sidelobe levels as those obtained when using narrow beams on transmit and receive depends on the array size, the spoiling factor used, and the pattern synthesis algorithm. These should be considered at the RPAR's design stage and is beyond the scope of this study. A larger and heavier aperture consuming more power requiring a pedestal that can support higher rotation speeds may increase the system cost, but this is dependent on the selection of R_F and is likely still more affordable than the four-faced MPAR. For example, for an RPAR with a two-way stationary 1° beamwidth when using narrow transmit–receive beams, the aperture would need to be increased by ∼19% in azimuth for a spoiling factor of $F = 3$ if the resolution is to be maintained (i.e., the transmit–receive combination results in an effective beamwidth of 1°). And finally, the sensitivity loss could be recovered by increasing the power radiated by each array element or alternatively using longer pulse-compression waveforms. For example, there is a sensitivity loss relative to the narrow beam of ∼6.2 dB when spoiling the transmit beam by a factor of 3, and ∼8.5 dB by a factor of 5 for the illustrative antenna patterns presented in Fig. 1. These sensitivity losses, which are greater than the theoretical loss of $10\log_{10}(F)$, result from the pattern synthesis technique used to produce the spoiled transmit beams used in the DB technique [33].

B. Variance Reduction

For the second possible application, the number of samples per CPI, the PRT, and the rotation speed are maintained at M, T_s, and ω. Similar to the previous scenario, operation is in a constant rotation regime, with R_F receive beams being digitally generated from each transmit beam. Receive beams are directed at approximately the same azimuth angle, since $\omega M T_s = \Delta\theta_1$ and are spaced exactly by $\Delta\theta_1$. Samples received on these beams can be coherently combined to obtain $M_{\mathrm{DB}} = M R_F$ samples. Thus, increasing the number of samples by the factor R_F can result in a significant reduction in the variance of radar-variable estimates [29]. The reduction factor depends on the dwell times and several signal characteristics, but it is mostly controlled by the signal-to-noise ratio (SNR), the spectrum width (σ_v), and the copolar correlation coefficient (ρ_{hv}), for the reflectivity and polarimetric-variable estimates. It is noted that at high SNR, the reduction factor is directly proportional to R_F and independent of width or other signal characteristics.

To illustrate the potential data quality improvement, Fig. 3 shows the SD of signal power estimates as a function of the number of samples, M, computed from simulated time-series data for a 10-cm wavelength radar with $T_s = 3$ ms (typically used in surveillance scans), $\sigma_v = 2$ ms^{-1}, and a maximum unambiguous velocity $v_a = 8.3$ ms^{-1}. A set of SNR are selected to account for the spoil factors ($F = 1$ or pencil, $F = 3$, $F = 5$) and the potential sensitivity reduction incurred when spoiling the transmit beam. SNRs of 2 and 20 dB are selected for the pencil beam ($F = 1$) as a reference, and SNRs for the spoiled beams are derived reducing those by the corresponding sensitivity loss (i.e., 6.2 dB for $F = 3$ and 8.5 dB for $F = 5$). The markers on each curve illustrate the potential reduction in the SD of power estimates for the application of DB with spoiled factors of 3 and 5, and with $0.5\theta_1$ sampling (i.e., $R_F = 5$ and $R_F = 9$, respectively), with respect to the pencil beam without using DB. Specifically, the circles on the curve show the SD of power estimates when using DB to improve data quality with $F = 3$ and $R_F = 5$, and the stars show the SD of power estimates with $F = 5$ and $R_F = 9$. At medium-to-high SNRs (>∼8 dB), a reduction of ∼0.5–1 dB in the SD of estimates can be achieved using DB. Even though this only shows the improvement for signal power estimates, increasing the number of samples also reduces the bias and SD of all spectral moments and polarimetric variables. The CONOPS presented by this application of the DB also exploits the RPAR beamforming capability, but now to reduce the variance of radar-variable estimates. In comparison with a similar pencil-beam CONOPS, this application would not require an increase in the rotation speed and has the potential of significantly reducing the fluctuation of estimates in the fields of radar products (and thus improving interpretation of the displayed fields).

These two applications of the DB technique may be highly suitable for observing different types of precipitation systems.

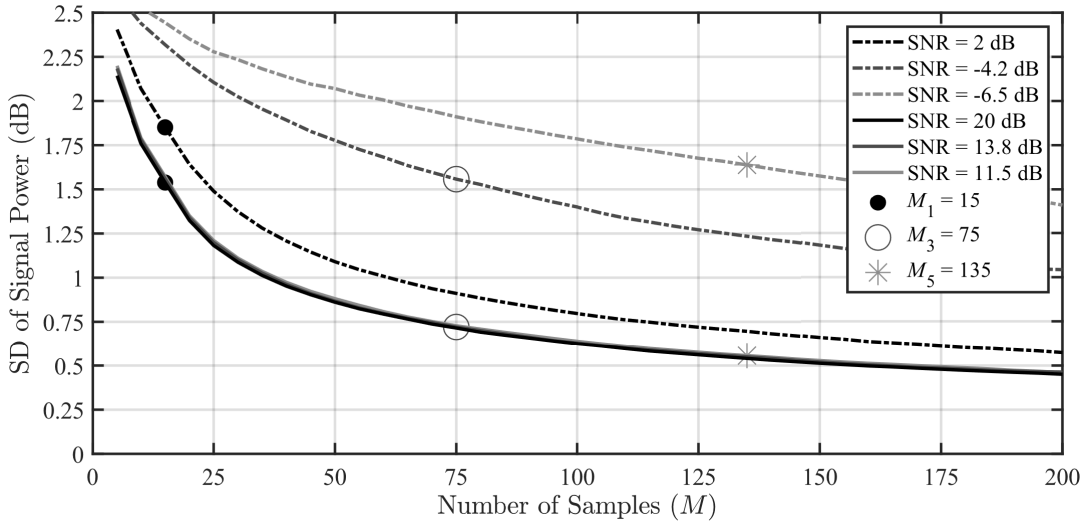

Fig. 3. SD of signal power estimates as a function of M for $T_s = 3$ ms, $\sigma_v = 2$ m s^{-1}, and several representative SNRs. The dot markers at $M_1 = 15$ represent the typical number of samples for the surveillance scan of VCP 212. Circle and star markers represent the number of samples obtained with DB for $\Delta\theta_1 = 0.5\theta_1$, and with $F = 3$ and $F = 5$, respectively.

That is, volume coverage patterns (VCPs) for observing fast-evolving convective precipitation systems could use the first application of the DB technique with its higher rotating speed, while VCPs for stratiform precipitation systems could use the second application collecting the higher number of samples realizing reduced weather data variance.

For example, consider the normal WSR-88D operational VCP number 212 for convective precipitation, which takes approximately 4.5 minutes to complete the operation [34]. An RPAR using II.A with a spoil factor $F = 1.5$, $R_F = 3$ ($\Delta\theta_1 = 0.5\theta_1$), and rotating three times faster than the WSR-88D could complete the VCP in about 1.5 min, maintaining the same variance of estimates using all of the same radar parameter constraints established for the operation. For this relatively small spoiling factor, it is expected that additional RPAR design considerations to account for the use of DB (under these assumptions) should not be very demanding. Alternatively, consider the VCP number 32 for clear-air or weak precipitation situations, which takes approximately 9.5 min to complete [34]. An RPAR using II.B with a spoil factor $F = 3$, $R_F = 5$ ($\Delta\theta_1 = 0.5$), and rotating at the same speed could complete the VCP in the same period, but there would be a significant reduction in the SD of estimates due to the increased number of samples ($\sim R_F^{1/2}$ at high SNR [29]). As noted, this is especially important for weak-signal precipitation VCPs where coherent processing of a large number of samples is required to detect and estimate signals with low SNR. Furthermore, given that these systems do not normally present strong reflectivity gradients, there would be little impact from the higher two-way pattern sidelobe levels. However, as discussed previously, spoiling the transmit beam does lead to a reduction in sensitivity (e.g.,$\sim$6.2 dB) which reduces the detectability of some of the weaker echoes. Nevertheless, the increase in number of samples results in variance reduction and facilitates the reduction in censoring thresholds that in turn partially compensates for the sensitivity loss. This can be seen in Fig. 3 by comparing the SD of power estimates in the black dot marker found on the solid line ($M_1 = 15$ at SNR $= 20$ dB) compared with the circle marker on the dotted line ($M_3 = 75$ at SNR $= -4.2$ dB) where the SNR is 6.2 dB lower, yet the SD of estimates of M_3 is better.

Of course, the limitations related to the use of spoiled transmit beams have to be considered for an operational use of the DB technique. That is, important aspects have to be considered in the design of the rotating pedestal and the antenna. Pedestals would be required to rotate the antenna at higher speeds (based on the scan-time reduction factor desired), and the antenna aperture would have to be increased so that the two-way sidelobes can be lowered (tapering the receive array) to meet the prescribed requirements. One alternative proposed for future research is to investigate the use of other beamforming methods in conjunction with the DB technique to reduce increased sidelobe levels. Both of these applications of the DB technique are possible and are illustrated in Section IV. The next section will advance the theoretical aspects of DB by presenting a practical implementation of the technique and discuss important antenna calibration considerations.

III. Practical Implementation, Calibration, and Verification of the DB Technique

A. Implementation on the ATD System

The recently installed ATD radar system at the NSSL in Norman, OK, is an active S-band planar dual-polarization PAR. It was funded jointly by the NOAA and the Federal Aviation Administration (FAA). It is being developed by the NSSL, the Cooperative Institute for Mesoscale Meteorological Studies (CIMMS) at the University of Oklahoma, MIT Lincoln Laboratory, and General Dynamics Mission Systems [14], [35], [36]. The antenna is composed of 76 panels, where each panel consists of an 8×8 set of radiating patch-antenna elements with dual linear polarization (H and V), for a total of 4,864 elements. The peak power for each antenna element

is 6 W per polarization, which results in ∼29 kW of peak transmit power. The system makes use of pulse compression to meet sensitivity and range-resolution requirements [37], [38], achieving a sensitivity of approximately 0 dBZ at 50 km. The antenna elements in the ATD have been spaced by half wavelength, which results in a ∼4 × 4 m aperture that produces a ∼1.58° beamwidth on broadside. On receive, the antenna is partitioned into overlapped subarrays (consisting of 8 panels each, 2 in azimuth by 4 in elevation) to produce lower sidelobes and suppress grating lobes outside of the main beam of the subarray pattern [39]. Through element-level control of the magnitude and phase of transmitted signals, this system is capable of synthesizing different beam patterns on transmission. Therefore, the ATD can be used to implement the DB technique in an experimental research environment. The DB technique was implemented in the ATD using $F = 3$ with $R_F = 3$ or 5 ($\Delta = 1$ or 0.5) and using $F = 5$ with $R_F = 5$ or 9 ($\Delta = 1$ or 0.5).

Initial array calibration was performed in the anechoic chamber at MIT Lincoln Laboratory, whereby individual element transmit powers and phases were measured. These measurements were used to derive lookup tables that digitally equalize the power of each element and align their phases. The next subsection provides important calibration considerations needed for an effective implementation of the DB technique.

B. Calibration of Power in DB Implementation

The spoiled transmit beams produced by the ATD are synthesized using phase-only coefficients to maximize the power on transmit [33]. The co-polar main lobes of these antenna patterns were measured using the calibration infrastructure installed in the vicinity of the ATD [40], and those corresponding to the horizontal polarization are shown in Fig. 4 (axes are scaled to enhance visual interpretation). Azimuth-plane measurements of the horizontal polarization broadside transmit beams, as well as the two-way beams resulting from the use of each of these transmit beams with narrow beams on reception are presented in Fig. 5. Note that two-way beams are normalized (for visual interpretation) using the highest peak in the set of digitally formed beams.

Examination of the two-way beams in Fig. 5(c) and (d) reveals variations in the magnitude of beam peaks. These beam peak differences arise as a consequence of the small ripples in the spoiled transmit beams [Fig. 5(a)], which have to be digitally compensated prior to DB processing. The beamwidth and peak-sidelobe level (PSL) of the two-way beams were measured and the results for the horizontal polarization are presented in Tables I and II, respectively. Similar results were obtained for the vertical polarization beams.

It is apparent from these measurements that the beamwidth is not constant and that two-way beams near the edge of the spoiled transmit beam's main lobe are narrower. This is due to the sharp decay in main-lobe energy (from the spoiled beam) on the digitally formed receive beams near the edges. Given that the beamwidth determines the resolution volume, where most of the main-lobe energy is concentrated, it is important to consider these variations for both the horizontal

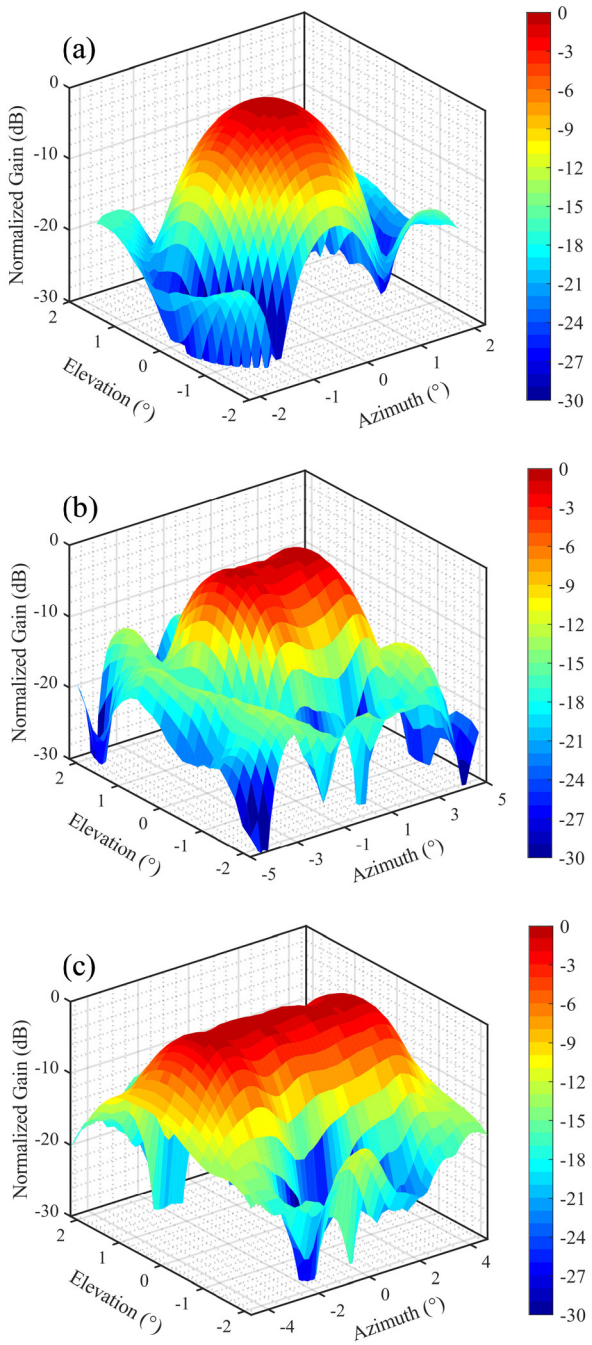

Fig. 4. Measured one-way normalized ATD antenna main-lobe transmit patterns. (a) Narrow beam, (b) beam spoiled by $F = 3$, and (c) beam spoiled by $F = 5$.

and vertical polarizations to produce accurate polarimetric measurements using the DB technique. It is also noted that the PSL increases significantly with the use of spoiled transmit beams. Specifically, the measurements indicate an average increase of approximately 17.52 dB for $F = 3$ and 21.88 dB for $F = 5$, both with respect to the narrow beam. The PSL of the two-way beams near the edges for negative azimuth angles appears to be consistently lower (for both $F = 3$ and $F = 5$). This is explained by observing that even though the narrow transmit beam (blue trace in Fig. 5(a) has good symmetry, the two-way narrow beam does not [Fig. 5(b)].

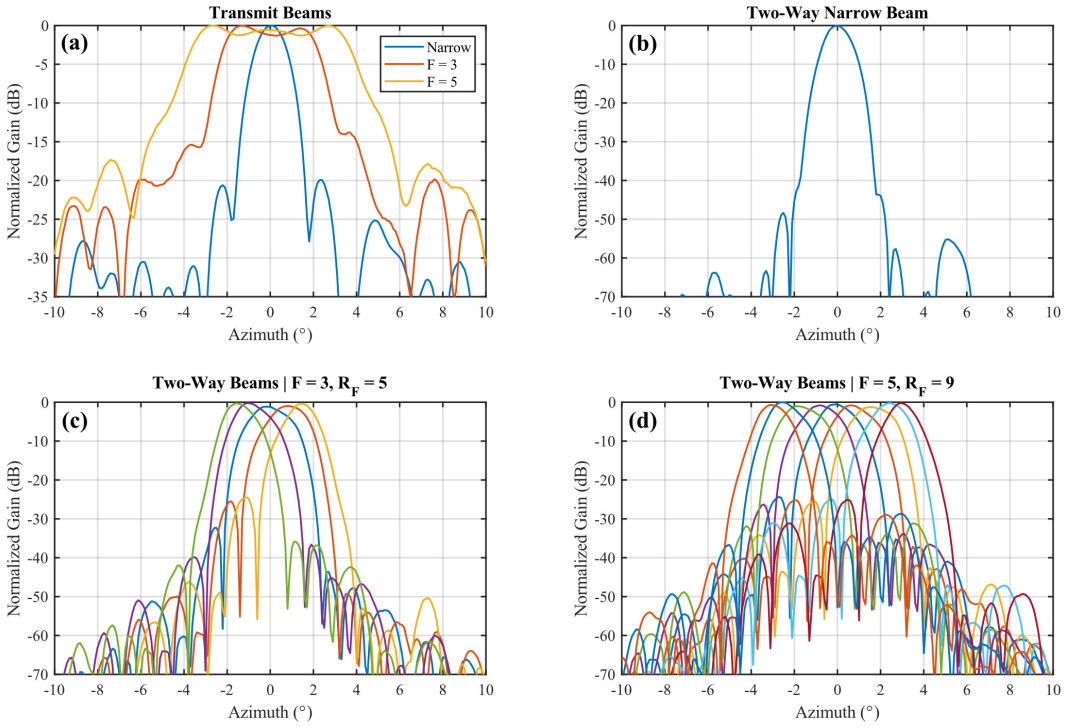

Fig. 5. Azimuth-plane measurements of ATD horizontal polarization antenna patterns on broadside (a) one-way transmit narrow and spoiled beams for $F = 3$ and $F = 5$, (b) two-way narrow beam, (c) two-way spoiled beams for $F = 3$ and $R_F = 5$, and (d) two-way spoiled beams for $F = 5$ and $R_F = 9$. For (c) and (d), the beam steering angles are computed for $0.5\theta_1$ sampling.

TABLE I

MEASURED ATD TWO-WAY ANTENNA PATTERN BEAMWIDTHS

Beam Type	Beamwidth (°)								
	φ_{-4}	φ_{-3}	φ_{-2}	φ_{-1}	φ_0	φ_1	φ_2	φ_3	φ_4
Narrow	—	—	—	—	1.58°	—	—	—	—
Spoiled F=3 and R_F = 5	—	—	1.75°	2.15°	2.32°	2.24°	1.76°	—	—
Spoiled F=5 and R_F = 9	1.87°	2.06°	2.42°	2.32°	2.23°	2.36°	2.39°	2.08°	1.77°

TABLE II

MEASURED ATD TWO-WAY ANTENNA PATTERN PEAK SIDELOBE LEVELS

Beam Type	Peak Sidelobe Level (dB)								
	φ_{-4}	φ_{-3}	φ_{-2}	φ_{-1}	φ_0	φ_1	φ_2	φ_3	φ_4
Narrow	—	—	—	—	-48.35	—	—	—	—
Spoiled F=3 and R_F = 5	—	—	-35.84	-36.62	-31.78	-25.49	-24.43	—	—
Spoiled F=5 and R_F = 9	-28.96	-28.68	-31.14	-26.33	-24.32	-25.19	-24.14	-24.67	-24.80

The appearance of the first sidelobe on the two-way narrow beam pattern at approximately $-2.6°$ in azimuth indicates that the one-way receive beam sidelobe levels are higher on the negative azimuth angles. As the one-way receive beam is digitally steered toward negative azimuth angles, the first sidelobe gets suppressed by the decaying main lobe on the spoiled transmit beam. The presence of this first sidelobe was confirmed by examining the one-way receive beam pattern (not shown here).

Power calibration for the DB technique was performed to ensure that the powers measured by receive beams in each polarization (H and V calibrated independently) are equal for the same target. Considering that this is a weather radar, a calibration procedure for volumetric targets was carried out. First, main-lobe (null to null) powers for the measured two-way beams [single cuts shown in Fig. 5(b)–(d)] were integrated in azimuth and elevation. Then, using the center beam as a reference and normalizing its integrated power to 0 dB, other beams were digitally compensated by the relative difference between their integrated main-lobe power with respect to that of the center beam. This ensures that the integrated powers of all main lobes are equal. The approach is

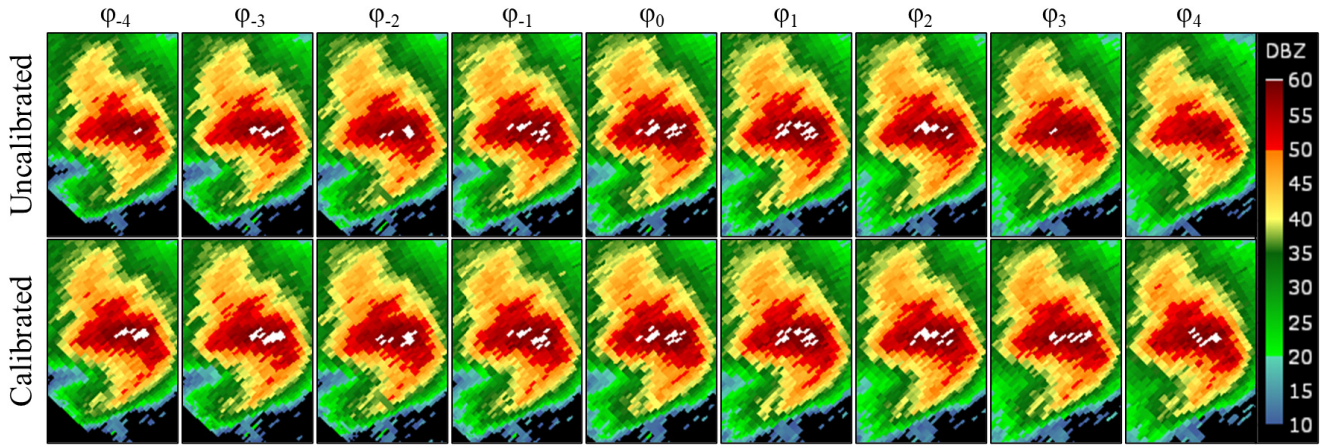

Fig. 6. Fields of reflectivity produced from two-way beams with $F = 5$ and $R_F = 9$. (Top row) uncalibrated and (Bottom row) calibrated.

similar to that discussed in [41] and [42], although main-lobe integrated powers are used here instead of beam peaks. Note that given the significant beamwidth variations (as presented in Table I), which leads to resolution volumes of different sizes, compensating with the two-way beam peak differences only would not be sufficient for distributed weather targets. Details about polarimetric calibration using the DB technique are not presented here and are left for future research.

The measurements presented in this subsection motivate the importance of accurate calibration of signal power to successfully implement the DB technique. The calibration procedure for signal phase is outlined in the next subsection.

C. Calibration of Phase in DB Implementation

In addition to correcting for signal power differences as a function of steering angle, the phases of the two-way beams may have to be aligned to ensure a coherent transition across the R_F receive beams for Doppler processing. Achieving phase calibration requires two considerations. First, similar to the power calibration, instantaneous phases of the two-way beam peaks were measured and digitally aligned. It consists of measuring signal phases at the peak of each of the two-way beams and deriving a set of phase alignment coefficients such that all two-way beam-peak phases are equal (arbitrarily set to 0° here). Then, phase alignment coefficients are applied digitally at the signal processor. Second, a deterministic phase difference arises because the antenna plane does not contain the center of rotation (due to the antenna arm used to attach the antenna to the pedestal, which displaces the antenna from the rotation center). That is, the phase centers for consecutive two-way DBs are shifted by

$$\delta_\theta = 2\pi \frac{d}{\lambda}[1 - \cos(\omega M_{\mathrm{DB}} T_s)] \ [\mathrm{deg}] \tag{2}$$

where d is the distance between the center of rotation and the array phase center, and λ is the radar wavelength. This deterministic phase compensation factor aligns the phase centers for the two-way DBs. It is noted that this depends on the particular RPAR design, and it may not be necessary if the antenna and the axis of rotation are in the same plane. Phase calibration is critical for the DB technique to achieve the scan-time reduction of R_F. If the phases of signals from DB samples are not coherent across two-way beam transitions, the combined time-series data cannot be coherently processed. Any loss of coherency from sample to sample would prevent the use of conventional pulse-pair or spectral processing methods (e.g., clutter filtering).

Calibration allowed the implementation of DB to demonstrate both applications proposed in Section II, namely: 1) scan time reduction and 2) variance reduction. The proof-of-concept implementation of the DB technique on the ATD allows for $F = 3$ or $F = 5$ with $R_F = 5$ or 9, respectively ($0.5\theta_1$ sampling), and a rotation speed of $\omega = 4$ or 8° s^{-1}. In addition, a narrow beam mode that mimics the operation of a reflector-antenna radar was implemented to validate the results from using the DB technique.

D. Verification of Implementation and Calibrations

Calibration is verified by digitally applying calibration corrections derived in II.B to volumetric weather targets. A sector scan was collected on March 27, 2020 at 18:07:45 Z, by commanding the ATD system to mechanically rotate clockwise from 300° to 340° in azimuth at $\omega_1 = 4°$ s^{-1}, and a constant 0.5° elevation angle. A total of 64 pulses were collected per CPI at a PRT of 3 ms, resulting in a $0.5\theta_1$ azimuthal sampling spacing. The broadside transmit beam was spoiled with $F = 5$, and $R_F = 9$ beams were generated for each polarization on reception. The data recording period for every pulse was set to capture samples from 100 to 450 μs, which correspond to ranges between 15 and 67.5 km.

Data from all receive beams observing the convective precipitation system were initially processed without applying calibration corrections. Fields of reflectivity produced for individual uncalibrated receive beams are shown in the top row of Fig. 6. Comparing the panels from either one of the edge beams (φ_{-4} and φ_4) with the center beam (φ_0), noticeable differences (~2–3 dB) can be seen in the estimated fields although the time lag between them is only 0.768 s. Differences for other receive beams are present as well, but they may not be as apparent in this qualitative comparison. Analogous fields of reflectivity derived by applying calibration

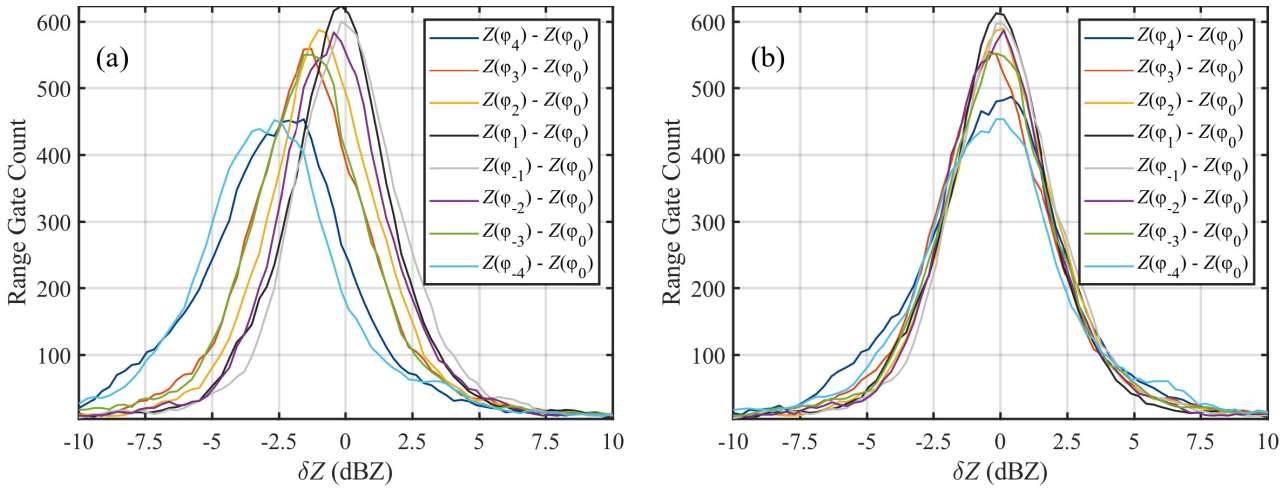

Fig. 7. Histograms of reflectivity differences (δZ) computed from gate-to-gate differences between reflectivity fields shown in Fig. 6. (a) Uncalibrated beams and (b) calibrated beams. Differences are computed with respect to the center beam, φ_0.

corrections are shown in the bottom row of Fig. 6. No qualitative differences are observed in reflectivity estimates from these panels, which corroborate the effectiveness of calibration corrections given that observations from all receive beams are similar.

A quantitative evaluation of calibration corrections is carried out to confirm these results. Gate-to-gate differences between reflectivity fields estimated from each beam (φ_i) with respect to the center beam (φ_0) are computed for the uncalibrated and calibrated cases to produce histograms of reflectivity differences (δZ), presented in Fig. 7. Considering the relatively slow evolution of the weather with respect to the time differences among these beams (<1 s), it is expected that δZ should be zero-mean with an SD roughly dictated by the radar's acquisition parameters (M and T_s) and signal characteristics (SNR and σ_v). Panel (a) shows the histograms of δZ for uncalibrated reflectivities, while panel (b) shows the same for calibrated reflectivities. Results in (a) show that, on average, receive beams φ_{-4} and φ_4 (which are symmetric about the broadside) are equally biased by ~ -2.5 dB, while other receive beams also present lower negative biases on average ($\sim$1.5 dB for $\varphi_{\pm 3}$, $\sim$0.7 dB for $\varphi_{\pm 2}$, and < 0.25 dB for $\varphi_{\pm 1}$). These negative biases are consistent with the power calibration corrections derived for the receive beams. Results in (b) verify the effectiveness of calibration corrections, as the histograms corresponding to all beams are centered more closely around zero with mean values < 0.054 dB.

To verify phase calibration, samples from a resolution volume containing a stationary point target were extracted from all nine two-way beams and were coherently processed to form a DB-CPI of 576 samples (9×64). These were used to estimate the targets' Doppler spectrum. The uncalibrated and calibrated spectra are shown in Fig. 8. Both phase corrections were applied to estimate the calibrated spectrum. It is apparent that phase discontinuities in the uncalibrated time-series IQ data result in the appearance of spurious harmonics, which are not present after phase calibration. In the next section, both DB applications are illustrated by scanning actual weather echoes and completing a quantitative analysis of the results.

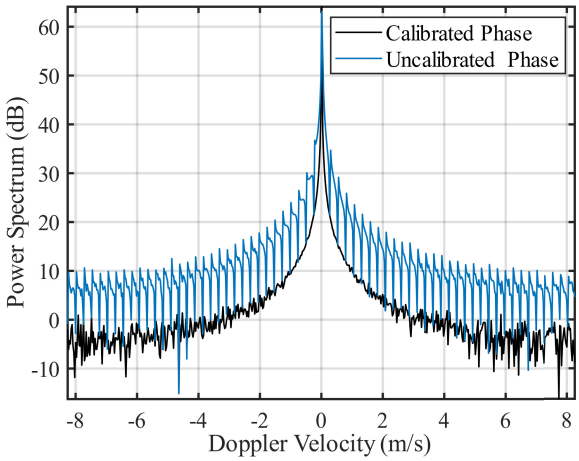

Fig. 8. Doppler spectra for the stationary point-target without phase calibration (blue curve) and with phase calibration (black curve).

IV. Demonstration of DB Applications

Implementation and testing of candidate research techniques on actual radar systems can provide significant practical value to consider an operational implementation of the proposed technique. After implementation and calibration of the DB technique, data were collected with the ATD system to demonstrate both applications proposed in Section II. Radar calibration parameters derived using the procedure described in Section III are applied in the digital signal processor for these demonstration experiments.

A. Experimental Sector Scans

For the first experiment, three sector scans were collected in rapid succession on March 19, 2020. For scan 1, the ATD rotated at $\omega_1 = 4^\circ$ s^{-1}, the broadside transmit beam was spoiled with $F = 3$, and $R_F = 5$ beams were generated for each polarization on reception. Data from this scan were collected at 17:48:54 Z, and are used to demonstrate the DB technique for data quality improvement (Section II.B). For scan 2, the ATD rotated at $\omega_2 = 4^\circ$ s^{-1}, both the transmit

and receive beams were broadside narrow, mimicking the operation of a conventional reflector-based radar. Data from this scan were collected at 17:49:46 Z, and are used here as a reference to verify the DB data. For scan 3, the ATD rotated at $\omega_3 = 8^\circ\ \mathrm{s}^{-1}$, the broadside transmit beam was spoiled with $F = 3$, and $R_F = 5$ beams were generated for each polarization on reception. Data from this scan were collected at 17:50:25 Z and are used to demonstrate the DB technique for scan time reduction by a factor of 2 (Section II.A). It should be noted that using $R_F = 5$ beams could allow a scan time reduction by a factor of 5, but that would require rotating five times faster, which was not possible at the time of this experiment. Thus, data from three two-way beams in scan 3 were discarded prior to DB processing to establish a fair performance comparison with scan 2. For all three scans, the radar broadside was commanded to mechanically rotate clockwise from 140° to 166° in azimuth, at constant 0.5° elevation, with a continuous pulse transmission at $T_s = 3$ ms. The settings for scans 1 and 2 result in 64 pulses for $0.5\theta_1$ sampling in azimuth, while settings for scan 3 result in 32 pulses for $0.5\theta_1$ sampling in azimuth since $\omega_3 = 2\omega_1$. Note that since $\Delta = 0.5$ for all scans, beam smearing effects (defined earlier as the fractional beamwidth increase) are equivalent on both scans. Specifically, the beamwidth of the ATD when using narrow pencil beams is 1.58°, which increases to approximately 1.64° when $\Delta = 0.5$. The average intrinsic ATD beamwidth of the 5 receive beams (see Table I) when using DB with $F = 3$ and $R_F = 5$ is 2.04°, which increases to approximately 2.13° when $\Delta = 0.5$. The data recording period for every pulse was set to capture samples from 200 to 600 μs, which correspond to ranges between 30 and 90 km. Receiver range-time samples were produced at a rate of 4 MHz, which results in a range sampling interval of 37.5 m.

Data from scans 1 and 3 were processed using the DB technique. That is, IQ data from two-way beams were calibrated in magnitude and phase and CPIs pointed in the same direction where grouped for processing. Radials of DB-CPIs from scan 1 resulted in 320 (5×64) IQ samples per range gate, while radials of data from scan 3 resulted in 64 (2×32) IQ samples per range gate. Data from scan 2 were processed using conventional signal processing techniques with radials of data with 64 IQ samples per range gate. Range-time processing was set to incoherently average samples from six consecutive range gates, which results in a range sampling spacing of 225 m. In addition, to exclude the impact of the wider beamwidth in scan 1 (with respect to scan 2), and strictly evaluate the improvement of the DB technique on scan 1 data, these data were reprocessed using the IQ samples collected with the broadside beam only (i.e., no DB and 64 IQ samples per range gate). Fields of radar-variable estimates resulting from processing the data from these scans are presented in Fig. 9. Panels are organized as follows: the top row corresponds to scan 1, the second row corresponds to the reprocessed scan 1 data using the broadside beam only, the third row corresponds to scan 2, and the bottom row corresponds to scan 3; the columns from left to right show fields of radar reflectivity (Z_h), differential reflectivity (Z_{DR}), differential phase (Φ_{DP}), and ρ_{hv}.

B. Demonstration of Variance Reduction

A qualitative comparison of radar-variable estimates from scans 1 and 2 is discussed first. While scan times were the same (∼6.5 s), the fields from scan 1 are spatially smoother compared with their scan 2 counterparts. This is a consequence of the combined effects of: 1) a reduction in the SD of estimates from the larger number of samples available for processing when using the DB technique and 2) a degradation in the spatial resolution of data collected with the DB technique (i.e., wider beamwidth), resulting from the use of spoiled transmit beams. Effects from 2) are excluded in the fields presented in the second row of Fig. 9, which were processed using IQ data from broadside beam in scan 1 only (although the transmit beam was spoiled by 3). Qualitative comparison of corresponding fields in the first and second rows of Fig. 9 confirms that there is a significant reduction in the variance of estimates when using the DB technique (first row). This is observed for all fields but is more noticeable in the fields of Z_{DR}. The smoothness of the field indicates a reduction in the SD of estimates. Also, comparing the fields of Z_h and Z_{DR}, it is apparent that power calibration for the DB technique was achieved since no data artifacts are observed, and estimates from scans 1 and 2 have comparable values. Comparison of the fields of Φ_{DP} from scans 1 and 2 indicates that phase calibration was also achieved successfully. Careful examination of the Z_h and Z_{DR} fields reveals what appears to be sidelobe contamination in the estimates from scan 1. This is observed in the Z_h and Z_{DR} fields from scan 1 in the area surrounding the strong Z_h core (∼57 dBZ) located to the south of the sector (indicated with white arrows in the panels of ρ_{hv}). This can also be inferred by comparing the fields of ρ_{hv} estimates, where lower signal cross correlation values (∼0.85–0.90) are observed in data from scan 1 around the suspected area with sidelobe contamination. This was expected, considering the significantly higher sidelobes on the two-way patterns resulting from the use of the spoiled transmit beams ($F = 3$), especially in the presence of a strong reflectivity gradient.

The spatial resolution appears to be slightly better on data from scan 2. This was also anticipated, considering the increased beamwidth of the two-way patterns resulting from the use of the spoiled transmit beam ($F = 3$). The ATD system was not designed to meet the beamwidth or sidelobe-level requirements specified in [2] using a narrow pencil beam and, consequently, it is even farther away from meeting these requirements when using this proof-of-concept implementation of the DB technique. Finally, a predicted sensitivity difference is observed by comparing the coverage of weather echoes in all radar variables. This difference appears to be smaller than the sensitivity loss from using a spoiled transmit beam and it is due to the increased number of samples obtained with the DB technique. That is, the performance of the coherency-based thresholding [43] technique in recovering valid weather measurements is improved by the increased number of samples. Since coherency-based thresholding is used to process both data sets, but more samples are available using the DB technique, more data that would otherwise have been filtered (i.e., without DB) are recovered.

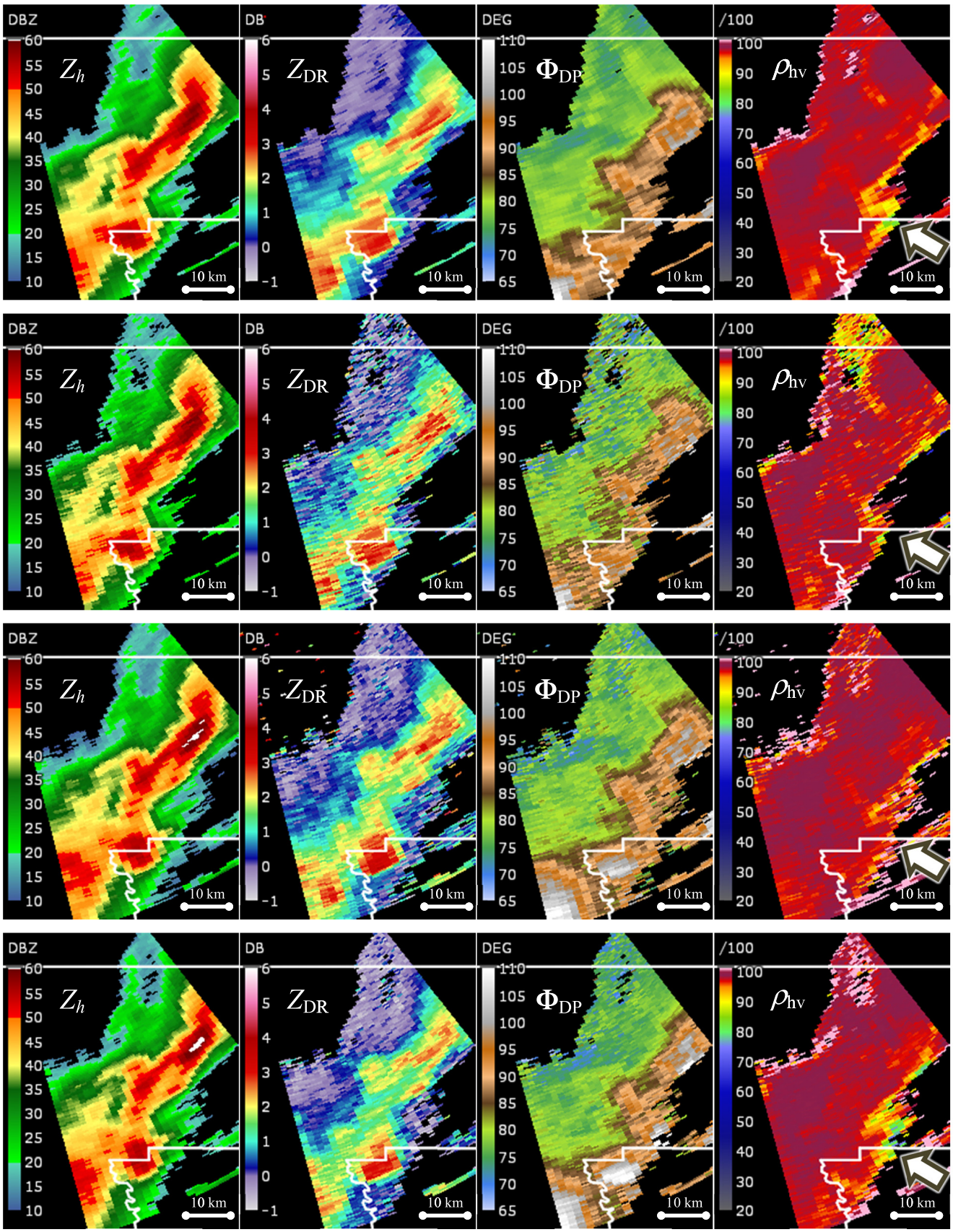

Fig. 9. Radar-variable estimates obtained from three scans collected in rapid succession. Panels are organized as follows: the top row corresponds to scan 1 (DB with $F = 3$, $R_F = 5$), the second row corresponds to the reprocessed scan 1 using the broadside beam only (DB with $F = 3$, $R_F = 1$), the third row corresponds to scan 2 (narrow beam), and the bottom row corresponds to scan 3 (DB with $F = 3$, $R_F = 2$); the columns from left to right show fields of radar reflectivity (Z_h), differential reflectivity (Z_{DR}), differential phase (Φ_{DP}), and copolar correlation coefficient (ρ_{hv}).

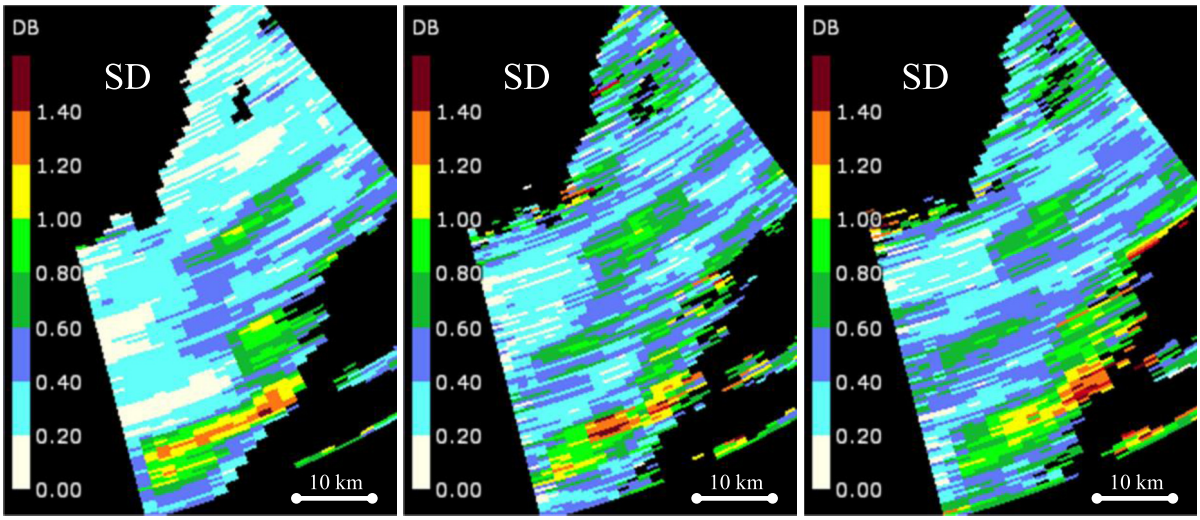

Fig. 10. Spatial fields of SD were produced using a running window of three beams in azimuth by three gates in range on the fields of Z_{DR} from Fig. 9. Comparing the left and center fields reveals the data quality improvement of the DB technique over the conventional processing and comparing the center and right fields shows that comparable data quality was achieved by scanning weather echoes twice as fast.

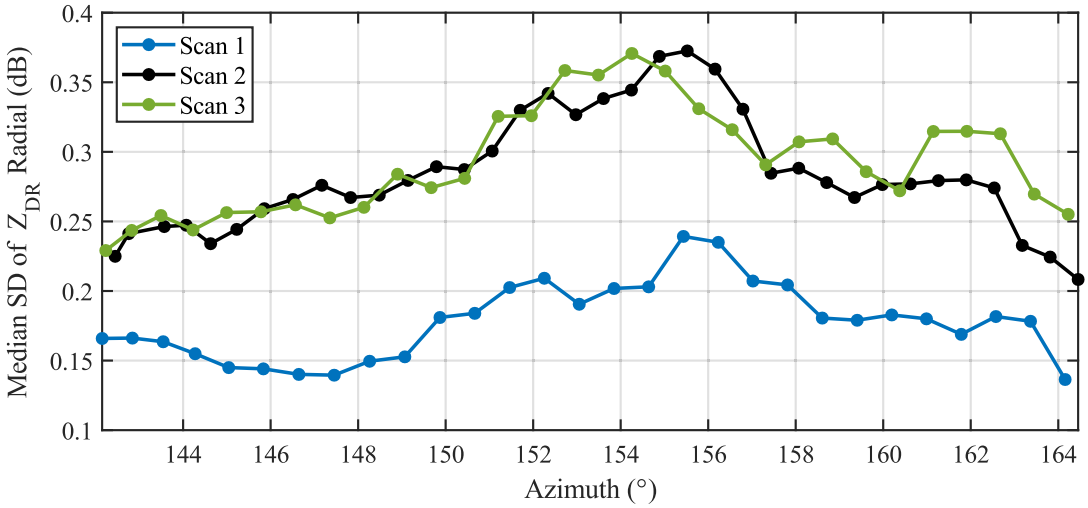

Fig. 11. Median spatial SD per radial of Z_{DR} as a function of azimuth. The blue, black, and green curves are from scans 1, 2, and 3, respectively.

C. Demonstration for Scan Reduction Times

Next, a comparison of radar-variable estimates from scans 2 and 3 is presented. Scan 3 data were collected in approximately 3.25 s, twice as fast as data from scan 2. Since data from scan 3 were collected at $\omega_3 = 8°\ \mathrm{s}^{-1}$, a set of $M = 0.5\theta_1/(\omega_3 T_s) = 32$ samples were obtained for every two-way beam. Using the DB technique with $R_F = 2$ and coherently combining IQ data from 2 beams pointed in approximately the same direction resulted in an effective CPI of 64 samples per radial. This CPI matches that of scan 2, and it is expected to result in similar data quality even though it was collected twice as fast. An analogous examination of radar-variable estimates confirms this hypothesis. That is, all fields have similar spatial texture, indicating that the SD of estimates is comparable. And while no data artifacts related to calibration are apparent, the region with suspected sidelobe contamination is present in data from scan 3, as expected. Possible ways to mitigate the impact on spatial resolution and sensitivity incurred by the use of spoiled transmit beams are provided in the conclusions.

To quantify the variance reduction as a result of using the DB technique, a spatial texture was derived from Z_{DR} fields. Spatial texture fields were produced using a running window of three beams in azimuth by three gates in range and computing the SD of estimates in the window. Comparing the left and center spatial SD fields in Fig. 10 reveals the data quality improvement of the DB technique over the conventional processing, while comparing the center and right spatial SD fields shows that data from scans 2 and 3 have comparable quality. Finally, Fig. 11 shows the median spatial SD per radial as a function of azimuth, where the blue, black, and green curves represent data from scans 1, 2, and 3, respectively. The average reduction in the SD of estimates for the results shown in Fig. 11 (i.e., the average of the ratio between the black and blue plots in linear units) is ∼1.58. Considering that the SD of estimates depends not only on the number of samples, but also on signal characteristics such as the SNR and σ_v, and assuming high SNRs, the lowest bound on the SD reduction factor would be 1 (i.e., no reduction for small σ_v) and the upper bound would be $(RF)^{0.5} \sim 2.23$ [29]. The SD reduction obtained here (for an actual range of SNRs and σ_v's)

is within the expected theoretical bounds and illustrates this application of the DB technique. It is clear from these results that a comparable spatial SD of estimates is achieved when using the DB technique described in Section II.A and that the spatial SD of estimates is significantly improved when using the DB technique in Section II.B. In Section V, a qualitative comparative analysis of DB data and WSR-88D data is presented.

V. Verification of DB data with KOUN radar

With the improvements of the DB technique in scan time or SD reduction illustrated in the previous subsection, data produced with this technique were verified by comparing them to a WSR-88D radar system. The KOUN radar in Norman, OK is operated and maintained by the NSSL and it is collocated with the ATD system. It serves as an experimental testbed for research and development of new techniques. Two simultaneous data collection experiments are presented for the verification process. The first one is used to evaluate the quality of spectral moments, namely Z_h, Doppler velocity (v), and σ_v. This case was selected because the Doppler velocities observed for this weather event did not exceed the maximum unambiguous velocity (v_a) on the scan from the ATD radar ($v_a = 8.27$ m s^{-1}). The second experiment was used to evaluate the quality of polarimetric variables, namely, Z_{DR}, Φ_{DP}, and ρ_{hv}. This case was selected because of the widespread nature of the weather event observed, which covered most of the sector observed with the ATD using the DB technique.

A. Experiment Comparing Quality of Spectral Moments

The first experiment was conducted on March 4, 2020. The ATD system was commanded to rotate at $\omega = 4°$ s^{-1}, the broadside transmit beam was spoiled with $F = 3$, and $R_F = 5$ beams were generated for each polarization on reception. Data from this scan were collected at 02:44:54 Z, as a stratiform precipitation system was advecting from the west and passing to the south of the radar site. The radar boresight was commanded to mechanically rotate clockwise from 150° to 175° in azimuth and at constant 0.5° elevation, with a continuous pulse transmission at $T_s = 3$ ms.

Similar to the first scan in the previous section, this scan resulted in 64 pulses for $0.5\theta_1$ sampling in azimuth. The data recording period for every pulse was set to capture samples from 400 μs to 1200 μs, corresponding to ranges of 60–180 km. Receiver range-time samples were produced at a rate of 4 MHz, which resulted in a range sampling interval of 37.5 m. The KOUN radar was following the operational VCP number 215, which commands to antenna system to rotate at 21.15° s^{-1} at the lowest elevation angle (0.5°). For this elevation, the CPIs from the surveillance scan consist of 30 samples at $T_s = 3$ ms^{-1}, with $0.5\theta_1$ azimuthal sampling of 0.5°, since the beamwidth of this system is approximately 1°. Data for the lowest elevation of the VCP were collected with the KOUN radar at 02:44:41 Z, and IQ data from the same azimuthal sector (i.e., 150° to 175°) were extracted for processing. Receiver range-time samples were produced at a rate of 0.6 MHz, which resulted in range sampling interval of 250 m.

There are several architectural differences between these two systems, the most relevant ones for this comparison being the antenna system and the scan strategies. However, with access to the received IQ data from both systems, the signal processing can be modified to compensate some system differences for a more fair data quality comparison. First, azimuthal resolution can be made equal by considering the impact of the rotation rate on the antenna patterns. That is, the *effective antenna pattern* [30] of an antenna rotating at uniform rate can be derived considering the displacement of resolution volumes for every sample in the CPI. This effective pattern defines an effective beamwidth that determines the azimuthal resolution of the data.

Considering the previously mentioned radar parameters for the KOUN radar, it was determined through simulations that to increase KOUN's effective beamwidth to ∼1.58° (and thus match the ATD beamwidth), the samples per CPI should be increased to $M_{KOUN} = 38$. Since the number of samples per CPI from each two-way receive beam (i.e., prior to applying DB processing) from the ATD was 64, 24 samples were discarded to get $M_{ATD} = 38$. Range-time processing was set to use only the third out of every six samples in range, resulting in a range resolution of 225 m but without increasing the effective number of samples through averaging. Finally, azimuthal sampling of data was set to 0.79° for $0.5\theta_1$ sampling. The second-order differences such as radar frequency (both are S-band radars), sensitivity, sidelobe levels, elevation beamwidth, and antenna height with respect to the ground were neglected for this comparison.

Data from these scans were processed with the considerations described, and the DB technique was used on data from the ATD system to improve the data quality. Radar-variable estimates from these scans are presented in Fig. 12. Panels are organized as follows: the top row corresponds to data from the KOUN radar, while the bottom row corresponds to the data from the ATD radar; columns from left to right show fields of estimated Z_h, v, and σ_v.

A comparison of corresponding estimates from both radars indicates that despite system differences, fields appear to be very similar to data from the ATD radar having superior SD due to the large number of samples ($5 \times 38 = 190$) per CPI produced by the DB technique. Comparison of v fields shows that velocities from the ATD data estimated using the DB technique are qualitatively similar to velocities estimated from the KOUN data. This provides evidence of accurate phase calibration on the DB data, which comprises alignment of instantaneous two-way beam-peak phases and phase correction for the shifted antenna phase centers.

Also, estimates of σ_v from the ATD using the DB technique appear to have significantly lower SD. That is, while the σ_v field estimated from KOUN data has a noisy texture (indicating a larger SD of estimates), estimates from the ATD data result in a smoother texture, creating a field that is easier to interpret. Accurate estimation of σ_v is typically challenging, especially for narrow spectra [44]. The increased number of available samples obtained with the DB technique seems to significantly improve the performance of the estimator. Examining the Z_h estimates from ATD data reveals no apparent evidence of sidelobe contamination. This was

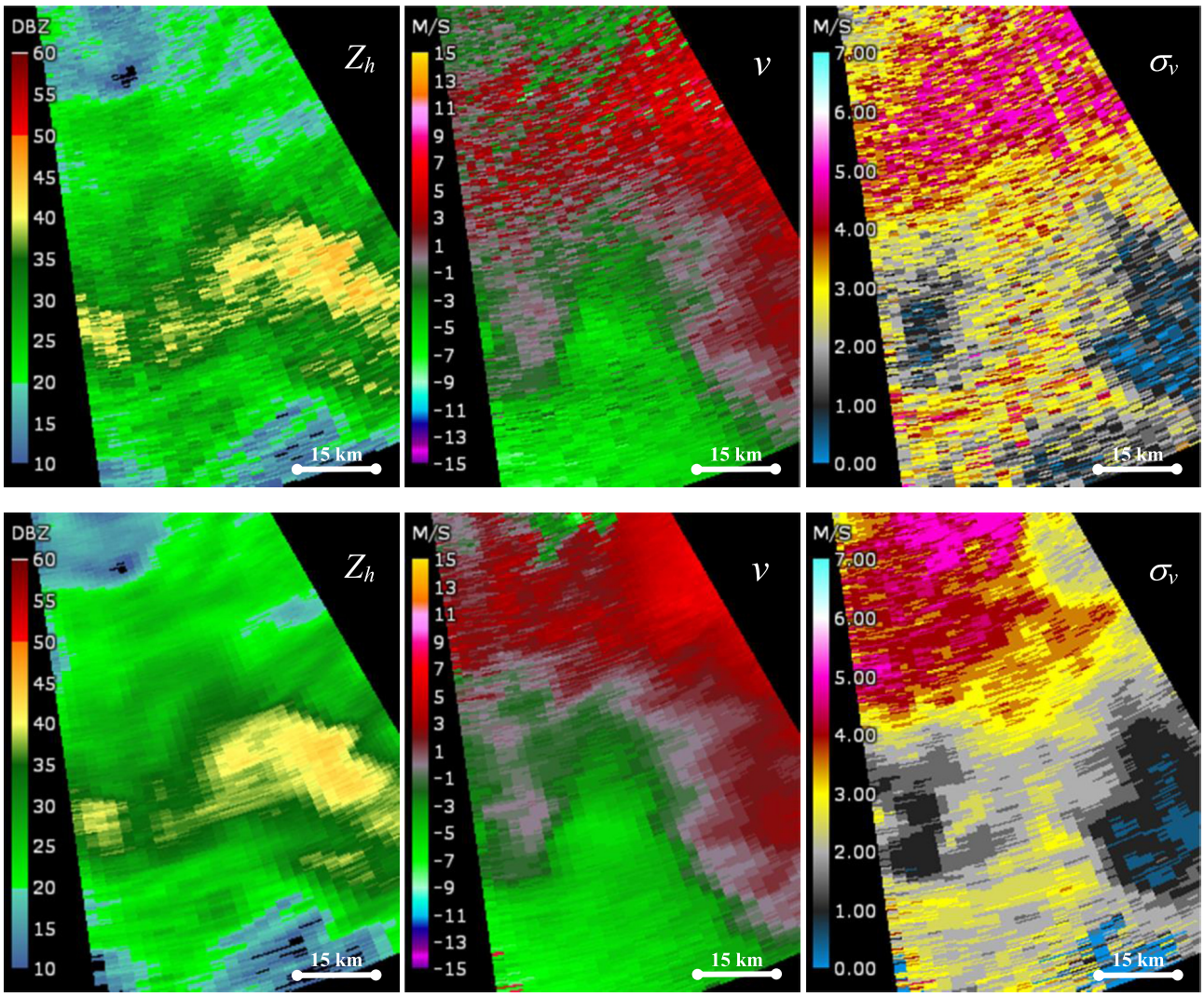

Fig. 12. Radar-variable estimates from weather echoes observed on March 4, 2020 with (top) the KOUN radar, and (bottom) the ATD radar using the DB technique with $F = 3$ and $R_F = 5$. Columns from left to right show fields of estimated Z_h, v, and σ_v.

expected given that the observed precipitation system does not present strong reflectivity gradients that would result in sidelobe contamination. While the sensitivity of the KOUN radar is superior than that of the ATD radar using a beam with $F = 3$ by ~13 dB (~7.5 dB for two-way narrow beam), it appears that there is no appreciable sensitivity impact on these data.

B. Experiment Comparing Quality of Polarimetric Variables

The second experiment occurred on November 20, 2019. The ATD system was commanded to rotate at $\omega = 4°\ s^{-1}$, the broadside transmit beam was spoiled with $F = 5$, and $R_F = 9$ beams were generated for each polarization on reception. Data from this scan were collected at 20:48:26 Z as widespread weak precipitation system was approaching the radar site from the west. The radar boresight was commanded to mechanically rotate clockwise from 260° to 280° in azimuth and at constant 0.5° elevation, with a continuous pulse transmission at $T_s = 3$ ms. Similar to the previous scans presented, this resulted in 64 transmit pulses for $0.5\theta_1$ sampling in azimuth. The data recording period for every pulse was set to capture range-time samples from 100 to 1000 μs, corresponding to ranges from 15 to 150 km. Similar to the previous case, the KOUN radar was following the operational VCP number 215. Data for the lowest elevation of the VCP were collected with the KOUN radar at 20:48:42 Z, and IQ data from the same azimuth sector (i.e., 260° to 280°) were extracted for processing. All other data recording and processing settings are the same as the ones described previously in this subsection.

Data from these scans were processed with the considerations described, and the DB technique was used on data from the ATD system to improve the data quality. Radar-variable estimates from the KOUN scan are presented in Fig. 13, and corresponding ones from the ATD scan are presented in Fig. 14. Panels for both figures are organized as follows: top-left shows fields of estimated Z_h (for reference), top-right shows Z_{DR}, bottom-left shows Φ_{DP}, and bottom-right shows ρ_{hv}. Similar to the analysis for the spectral moments, estimates from both radars appear to be very similar, but data from the ATD radar have superior quality due to the larger number of samples ($9 \times 38 = 342$) per CPI produced by the

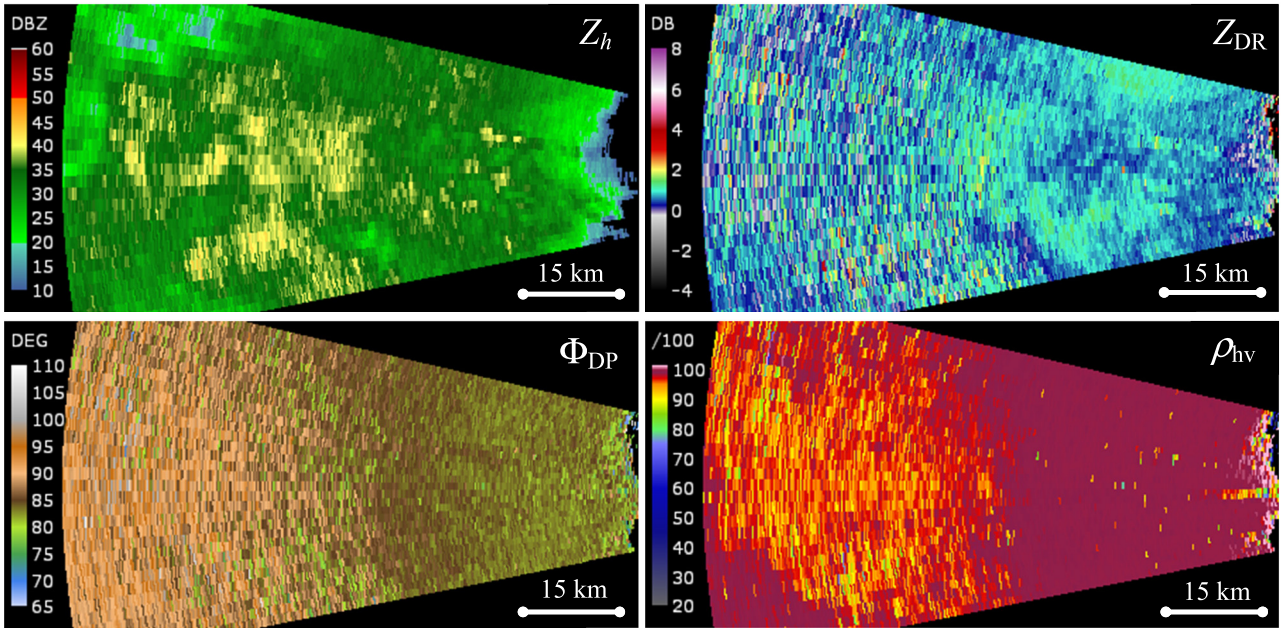

Fig. 13. Radar-variable estimates from weather echoes observed on November 20, 2019 at 20:48:42 Z with the KOUN radar: Z_h (top left), Z_{DR} (top right), Φ_{DP} (bottom left), and ρ_{hv} (bottom right).

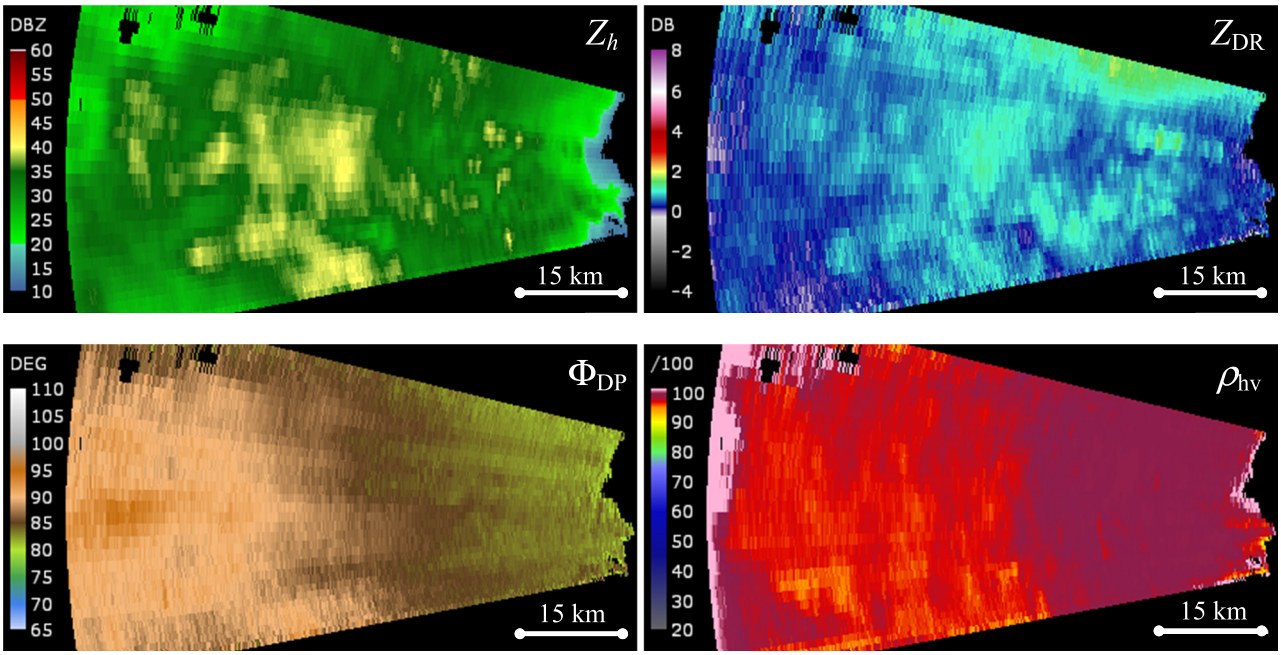

Fig. 14. Radar-variable estimates from weather echoes observed on November 20, 2019 at 20:48:26 Z with the ATD radar using the DB technique with $F = 5$ and $R_F = 9$: Z_h (top-left), Z_{DR} (top-right), Φ_{DP} (bottom-left), and ρ_{hv} (bottom-right).

DB technique. Examination of corresponding Z_{DR} fields shows good agreement in the mean value of estimates up to a range of ∼102 km. Beyond that range, estimates from KOUN data have very poor quality (i.e., high measurement errors), which lowers the value of these data for posterior interpretation or quantitative precipitation estimation processing. This is because polarimetric-variable estimates are more sensitive to measurement noise, and higher SNRs are necessary to achieve the precision levels required (SNR ∼ 8–10 dB).

Despite the large sensitivity difference between these radars, the additional reduction of SD achieved by the DB technique allows for more precise estimation of the Z_{DR} field for most of the observed sector. Similarly, there is good agreement between corresponding Φ_{DP} and ρ_{hv} fields, with the ATD data using the DB technique showing superior quality at low SNR (past ∼102 km in range). There is a small sensitivity difference observed far down range (∼135–150 km), where weak echoes in the Z_h field are censored on the ATD data, and ρ_{hv} estimates become invalid (i.e., $\rho_{hv} > 1$).

The analysis presented in this section shows great promise for the DB application for data quality improvements when observing stratiform precipitation systems, where sidelobe

contamination is unlikely to be present and spatial resolution is not critical. The increased number of samples available to estimate spectral moments and polarimetric variables provides fields with visibly less noisiness, which could potentially enhance interpretation and posterior processing of the radar base data.

VI. Conclusion

Meeting the demanding *Optimal Functional Requirements* introduced in the NOAA/NWS requirements for future weather surveillance radar will require exploiting capabilities of advanced radar systems. The RPAR architecture may be an affordable candidate that meets threshold requirements and proper CONOPS solutions can be expected to meet some of the optimal requirements that NOAA/NWS has targeted. By exploiting a PAR's unique dynamic capabilities in conjunction with the application of advanced signal processing techniques, it is possible to design an RPAR CONOPS capable of reducing scan times and/or the variance of radar-variable estimates. The DBs technique presented in this article could provide a way to reduce the RPAR scan times and achieve the required volumetric update times ($\sim$1 min), or reduce the variance of estimates to the desired level, or a combination of both. Other digital beamforming techniques have been proposed for RPAR systems; however, the novelty of the DB technique is that it allows the coherent combination and processing of CPIs from different receive beams, and it is the first demonstration of digital beamforming in azimuth using dual-polarization weather RPAR. The DB technique was introduced in Section II, and two new CONOPS applications for it were described, namely, the scan time (II.A) and the variance (II.B) reduction techniques. The two-way beam patterns for the narrow and spoiled transmit beams were characterized in terms of the spatial resolution (beamwidth and peak sidelobe levels) in Section III. These measurements were used to quantify the impact of using spoiled transmit beams on the data quality and to provide a calibration procedure for the implementation and testing of the technique. Power calibration for the DB technique was verified by scanning meteorological volume targets and showing that the power distributions of calibrated two-way beams were unbiased. Phase calibration for the DB technique was verified by scanning an external stationary point target and comparing the measured phases of two-way beams prior-to and post applying the calibration procedure. Section IV provided experimental results of using the DB technique with the ATD radar. The first DB application is illustrated in Section IV-A by collecting two scans of data, one using a two-way narrow beam (for reference) rotating the PAR at $\omega = 4\ ^\circ\ \mathrm{s}^{-1}$, and the other using the DB technique and collecting comparable data twice as fast. The second application is illustrated in Section IV.B by collecting two scans of data, one using a two-way narrow beam (for reference) rotating the PAR at $\omega = 4\ ^\circ\ \mathrm{s}^{-1}$, and the other using the DB technique which produced visibly smoother fields of radar products. While some evidence of apparent sidelobe contamination was observed when using spoiled transmit beams, this was expected considering that the ATD radar was not designed to achieve required sidelobe levels when using spoiled transmit beams.

An essential step to validate the performance of the DB technique was presented in Section V, where data from a collocated WSR-88D radar (KOUN) were collected simultaneously with the ATD using the DB technique. While these systems are different, a procedure for a fairer comparison was used and described in Section V. Two cases were presented to compare the quality of spectral moments and polarimetric variables. Qualitative results show a high degree of agreement between the fields of radar variables produced by processing the data from these systems, with the ATD fields (produced using the DB technique) exhibiting improved spatial textures. In particular, polarimetric-variable estimates were shown to greatly benefit from the variance reduction when using the DB technique. Finally, no impact from higher sidelobe levels was observed on these cases (as expected), since these stratiform precipitation systems did not present high reflectivity gradients.

Considering electronic steering capabilities of the RPAR, it may be more convenient to electronically scan in elevation (and mechanically in azimuth). Under this operating mode, beam steering biases typical in PARs [45] have to be corrected for accurate polarimetric measurements. Nevertheless, since the beam will remain in the vertical principal plane when using the DB technique, it is expected that copolar beam steering biases can be corrected through a calibration procedure similar to the one presented in this article and that cross-polar contamination will not introduce significant biases. This is supported by the results presented in [46], which show that measurement biases from copolar and cross-polar patterns are the lowest along the principal planes and that one-way cross-polar pattern powers in both H and V are below -60 dB along them. The DB technique could also be used to scan steering angles away from both principal planes; however, an effective polarimetric-calibration procedure would be required to achieve the required estimate accuracies. We note that this is not a limitation of the DB technique, but a much broader challenge in polarimetric PAR calibration for which mitigation schemes are currently being investigated.

Results presented show that the DB technique can be used to reduce the scan time or the variance of radar-variable estimates, at the expense of degraded sensitivity and spatial resolution (i.e., beamwidth and sidelobe levels) compared with two-way narrow pencil beams formed with the same RPAR. A possible way to mitigate the degradation in spatial resolution is to design an aperture that meets the beamwidth requirements when using narrow beams and increase the size of the receive aperture only to lower sidelobe levels of two-way beams using spoiled transmit tapers. Another alternative is to define an operational mode in which spatial resolution and sensitivity degradations resulting from the use of the DB technique are an acceptable tradeoff to reduce the scan time or the variance of radar-variable estimates. Possible ways to mitigate the sensitivity reduction include increasing the element peak transmit power or using longer pulse-compression waveforms. Another limitation of the technique involves the azimuthal rotation speed. That is, to achieve large scan-time reduction factors using the DB technique, azimuthal rotation speed has to be increased by the desired reduction factor. Considering the mechanical rotation machinery has a high

technology-readiness level, achieving higher rotation speeds with this well-known pedestal technology reduces the risk of designing, building, and deploying RPAR systems with higher rotation rates. Achieving high reduction factors (e.g., $R_F = 5$) may be the challenging point due to the required rotation speeds, consider that an operational implementation can be designed using a small time-reduction factor (e.g., $R_F = 2$). This relatively low increase in the rotation speed increase would bring a significant reduction in the scan time, with relatively modest demands on mechanical rotators. This would reduce the relative increase in the aperture size required to meet two-way sidelobe requirements given that a narrower spoiled transmit beam would be used.

An important and unique aspect to consider for the deployment of an RPAR is the increase of reflections coming from a water-coated radome. While spherical radomes may be the most suitable candidate for the RPAR because of the symmetric properties of the geometry, they may reflect part of the transmit beam energy on the array when the electronically steered beams reach angles far from the broadside (e.g., $>20°$, depends on the array geometry). Internal reflections levels at that point could increase by several decibels since the water layer on the radome increases the radome backscattering cross section. A direct implementation of the DB technique as presented in this article with the transmit beam always on broadside would reduce the risk of these array-damaging reflections when operating under a wet-radome regime with a spherical radome.

The DB technique may allow an RPAR-based CONOPS to meet the demanding requirements for the future weather surveillance network if the aforementioned tradeoff compromises are accounted for in the radar design process. Future PARs that are specifically designed to exploit the use of spoiled transmit beams should account for the increased two-way sidelobe levels to meet the requirements. While this may require increasing the aperture, it also allows for advanced techniques (such as DB) that support meeting the demanding requirements with an affordable architecture (compared with the stationary four-faced PAR). Future research efforts should investigate alternative modes for using the DB technique, and their associated tradeoff considerations (e.g., sidelobe levels, sensitivity loss) should be thoroughly quantified. Additional research plans for the RPAR CONOPS include the implementation of a motion-compensated steering technique, by which beams will be continuously electronically steered by a small angle to maintain a tracking point on the center of the resolution volume that is being sampled, and better support its integration with the DB techniques. This would exploit PARs beam agility and also mitigate beam-smearing effects, enhancing the CONOPS and allowing both a scan time reduction while maintaining data quality and spatial resolution (of a stationary PAR). It is expected that the outcome of these research efforts will continue to provide valuable information that can support the next design of the future U.S. weather surveillance radar network.

ACKNOWLEDGMENT

The authors would like to thank D. Zrnić (NOAA-NSSL), I. R. Ivić (OU-CIMMS), A. Kusmanoff (OU-JHLP), H. Thomas (MIT-LL), J. Kurdzo (MIT-LL), A. Morris (MIT-LL), and anonymous reviewers for useful discussions and comments that improved this article. They would like to thank the entire ATD team. They would also like to thank C. Schwarz (University of Oklahoma, CIMMS), D. Wasielewski (NOAA-NSSL), R. Mendoza (NOAA-NSSL), and John "Chip" Murdock (GD-MS), for the support in configuring and operating the ATD.

REFERENCES

[1] K. Hondl and M. Weber, "NOAA's meteorological phased array radar research program," in *Proc. IEEE Int. Symp. Phased Array Syst. Technol. (PAST)*, Oct. 2019, pp. 1–6.

[2] D. L. B. Blvd, "Radar functional requirement," NOAA/NWS, Norman, OK, USA, 2015. [Online]. Available: https://www.roc.noaa.gov/WSR88D/PublicDocs/NOAA_Radar_Functional_Requirements_Final_Sept%202015.pdf

[3] D. S. Zrnic and A. V. Ryzhkov, "Polarimetry for weather surveillance radars," *Bull. Amer. Meteorol. Soc.*, vol. 80, no. 3, pp. 389–406, Mar. 1999.

[4] J. M. Straka, D. S. Zrnić, and A. V. Ryzhkov, "Bulk hydrometeor classification and quantification using polarimetric radar data: Synthesis of relations," *J. Appl. Meteorol.*, vol. 39, no. 8, pp. 1341–1372, Aug. 2000.

[5] H. S. Park, A. V. Ryzhkov, D. S. Zrnić, and K.-E. Kim, "The hydrometeor classification algorithm for the polarimetric WSR-88D: Description and application to an MCS," *Weather Forecasting*, vol. 24, no. 3, pp. 730–748, Jun. 2009.

[6] M. R. Kumjian and A. V. Ryzhkov, "Polarimetric signatures in supercell thunderstorms," *J. Appl. Meteorol. Climatol.*, vol. 47, no. 7, pp. 1940–1961, Jul. 2008.

[7] D. S. Zrnic *et al.*, "Agile-beam phased array radar for weather observations," *Bull. Amer. Meteorol. Soc.*, vol. 88, no. 11, pp. 1753–1766, Nov. 2007.

[8] M. E. Weber, J. Y. N. Cho, J. S. Herd, J. M. Flavin, W. E. Benner, and G. S. Torok, "The next-generation multimission U.S. surveillance radar network," *Bull. Amer. Meteorol. Soc.*, vol. 88, no. 11, pp. 1739–1752, Nov. 2007.

[9] S. M. Torres *et al.*, "Adaptive-weather-surveillance and multifunction capabilities of the national weather radar testbed phased array radar," *Proc. IEEE*, vol. 104, no. 3, pp. 660–672, Mar. 2016.

[10] T.-Y. Yu, M. B. Orescanin, C. D. Curtis, D. S. Zrnić, and D. E. Forsyth, "Beam multiplexing using the phased-array weather radar," *J. Atmos. Ocean. Technol.*, vol. 24, no. 4, pp. 616–626, Apr. 2007.

[11] P. L. Heinselman, D. L. Priegnitz, K. L. Manross, T. M. Smith, and R. W. Adams, "Rapid sampling of severe storms by the national weather radar testbed phased array radar," *Weather Forecasting*, vol. 23, no. 5, pp. 808–824, Oct. 2008.

[12] K. A. Wilson, P. L. Heinselman, C. M. Kuster, D. M. Kingfield, and Z. Kang, "Forecaster performance and workload: Does radar update time matter?" *Weather Forecasting*, vol. 32, no. 1, pp. 253–274, Feb. 2017.

[13] C. A. Kerr and X. Wang, "Ensemble-based targeted observation method applied to radar radial velocity observations on idealized supercell low-level rotation forecasts: A proof of concept," *Monthly Weather Rev.*, vol. 148, no. 3, pp. 877–890, Mar. 2020.

[14] J. E. Stailey and K. D. Hondl, "Multifunction phased array radar for aircraft and weather surveillance," *Proc. IEEE*, vol. 104, no. 3, pp. 649–659, Mar. 2016.

[15] M. E. Weber, "Meteorological phased array radar research at NOAA's national severe storms laboratory," in *Proc. IEEE Int. Conf. Microw., Antennas, Commun. Electron. Syst. (COMCAS)*, Nov. 2019, pp. 1–6.

[16] B. Palumbo and A. Cucci, "Array antenna with multiple, independently scanned beams for a 3D radar," in *Proc. Antennas Propag. Soc. Int. Symp.*, 1977, pp. 1–2. [Online]. Available: https://doi-org.ezproxy.lib.ou.edu/10.1109/APS.1977.1147771

[17] B. Palumbo, "Some examples of systems developments in Italy based on phased array technology," in *Proc. Int. Symp. Phased Array Syst. Technol.*, Oct. 1996, pp. 444–449.

[18] E. Brookner, "Phased array radars-past, present and future," in *Proc. RADAR*, 2002, pp. 104–113.

[19] E. Yoshikawa *et al.*, "MMSE beam forming on fast-scanning phased array weather radar," *IEEE Trans. Geosci. Remote Sens.*, vol. 51, no. 5, pp. 3077–3088, May 2013.

[20] B. Isom *et al.*, "The atmospheric imaging radar: Simultaneous volumetric observations using a phased array weather radar," *J. Atmos. Ocean. Technol.*, vol. 30, no. 4, pp. 655–675, Apr. 2013.

[21] T. Ushio *et al.*, "Development and observation of the phased array radar at X band," in *Proc. 31st URSI Gen. Assem. Sci. Symp. (URSI GASS)*, Aug. 2014, pp. 1–4.

[22] J. M. Kurdzo *et al.*, "Observations of severe local storms and tornadoes with the atmospheric imaging radar," *Bull. Amer. Meteorol. Soc.*, vol. 98, no. 5, pp. 915–935, May 2017.

[23] K. A. Orzel and S. J. Frasier, "Weather observation by an electronically scanned dual-polarization phase-tilt radar," *IEEE Trans. Geosci. Remote Sens.*, vol. 56, no. 5, pp. 2722–2734, May 2018.

[24] O. Adrian, "M3R AESA technology for extended air defence," in *Proc. IEEE Radar Conf.*, May 2008, pp. 1–6.

[25] D. Schvartzman and S. M. Torres, "Distributed beams: A technique to reduce the scan time of an active rotating Phased Array Radar system," in *Proc. 100th Amer. Meteorol. Soc. Annu. Meeting*, 2020, pp. 1–10. [Online]. Available: https://ams.confex.com/ams/2020Annual/mediafile/Manuscript/Paper365842/Distributed%20Beams%20-%20Extended%20Abstract.pdf

[26] V. Kluckers, "Beam-shaping with active phased array radars," in *Proc. Int. Conf. Radar*, Sep. 2008, pp. 177–182.

[27] H. L. Van Trees, *Optimum Array Processing: Part IV of Detection, Estimation, and Modulation Theory*. Hoboken, NJ, USA: Wiley, 2004.

[28] F. Nai, "On the potential of adaptive beamforming for phased-array weather radar," Ph.D. dissertation, School Elect. Comput. Eng., Univ. Oklahoma, Oklahoma City, OK, USA, 2017, p. 209. [Online]. Available: https://shareok.org/handle/11244/48164

[29] R. Doviak and D. S. Zrnic, *Doppler Radar and Weather Observations*. Mineola, NY, USA: Dover, 2006.

[30] D. S. Zrnic and R. J. Doviak, "Effective antenna pattern of scanning radars," *IEEE Trans. Aerosp. Electron. Syst.*, vol. AES-12, no. 5, pp. 551–555, Sep. 1976.

[31] M. C. Leifer, V. Chandrasekar, and E. Perl, "Dual polarized array approaches for MPAR air traffic and weather radar applications," in *Proc. IEEE Int. Symp. Phased Array Syst. Technol.*, Oct. 2013, pp. 485–489.

[32] R. J. Mailloux, *Phased Array Antenna Handbook*. Norwood, MA, USA: Artech House, 2017.

[33] G. C. Brown, J. C. Kerce, and M. A. Mitchell, "Extreme beam broadening using phase only pattern synthesis," in *Proc. IEEE Workshop Sensor Array Multichannel Signal Process.*, Jul. 2006, pp. 36–39.

[34] *Federal Meteorological Handbook: Doppler Radar Meteorological Observations, Part C, WSR-88D Products and Algorithms*. 1991.

[35] M. D. Conway, D. D. Russel, A. Morris, and C. Parry, "Multifunction phased array radar advanced technology demonstrator nearfield test results," in *Proc. IEEE Radar Conf. (RadarConf)*, Apr. 2018, pp. 1412–1415.

[36] S. Torres *et al.*, "Towards an operational demonstration of the first full-scale polarimetric phased-array radar," in *Proc. 39th Int. Conf. Radar Meteorol.*, 2019, pp. 1–2.

[37] S. M. Torres, C. D. Curtis, and D. Schvartzman, "Requirement-driven design of pulse compression waveforms for weather radars," *J. Atmos. Ocean. Technol.*, vol. 34, no. 6, pp. 1351–1369, Jun. 2017.

[38] D. Schvartzman and S. Torres, "Design of practical pulse compression waveforms for polarimetric phased array radar," in *Proc. 39th Int. Conf. Radar Meteorol.*, 2019, pp. 1–9.

[39] J. S. Herd, S. M. Duffy, and H. Steyskal, "Design considerations and results for an overlapped subarray radar antenna," in *Proc. IEEE Aerosp. Conf.*, Mar. 2005, pp. 1087–1092.

[40] I. Ivić *et al.*, "An overview of weather calibration for the advanced technology demonstrator," in *Proc. IEEE Int. Symp. Phased Array Syst. Technol. (PAST)*, Oct. 2019, pp. 1–7.

[41] I. R. Ivić and D. Schvartzman, "A first look at the ATD data corrections. Preprints," in *Proc. 39th Int. Conf. Radar Meteorol.*, 2019, pp. 3–5. [Online]. Available: https://cscenter.co.jp/icrm2019/program/data/abstracts/Poster2-06_2.pdf

[42] I. R. Ivić and D. Schvartzman, "Weather calibration efforts on the advanced technology demonstrator," in *Proc. 100th Amer. Meteorol. Soc. Annu. Meeting*, 2020, pp. 2–8. [Online]. Available: https://ams.confex.com/ams/2020Annual/mediafile/Manuscript/Paper363084/ATD%20Calibration%20%28AMS%20Annual%202020%29%20Extended%20Abstract.pdf

[43] I. R. Ivić, D. S. Zrnić, and T.-Y. Yu, "The use of coherency to improve signal detection in dual-polarization weather radars," *J. Atmos. Ocean. Technol.*, vol. 26, no. 11, pp. 2474–2487, Nov. 2009.

[44] R. G. Frehlich and M. J. Yadlowsky, "Performance of mean-frequency estimators for Doppler radar and lidar," *J. Atmos. Ocean. Technol.*, vol. 11, no. 5, pp. 1217–1230, Oct. 1994.

[45] D. S. Zrnic, G. Zhang, and R. J. Doviak, "Bias correction and Doppler measurement for polarimetric phased-array radar," *IEEE Trans. Geosci. Remote Sens.*, vol. 49, no. 2, pp. 843–853, Feb. 2011.

[46] I. R. Ivić, "An approach to simulate the effects of antenna patterns on polarimetric variable estimates," *J. Atmos. Ocean. Technol.*, vol. 34, no. 9, pp. 1907–1934, Sep. 2017.

David Schvartzman (Member, IEEE) received the B.S. degree (*Summa Cum Laude)* in electrical and computer engineering from the National University of Asunción, Asunción, Paraguay, in 2011, and the M.S. and Ph.D. degrees in electrical and computer engineering from the University of Oklahoma, Norman, OK, USA, in 2015 and 2020, respectively.

He is a Research Scientist with the Cooperative Institute for Mesoscale Meteorological Studies, The University of Oklahoma, which is affiliated with the National Severe Storms Laboratory. As a member of the Advanced Radar Techniques Team, he develops evolutionary signal processing algorithms to improve quality, accuracy, and timeliness of phased array radars. He also works on calibration and integration of phased array radar systems and supports the development of algorithms for the operational U.S. WSR-88D network.

Dr. Schvartzman is an Adjunct Instructor with the University of Oklahoma School of Electrical and Computer Engineering, where he teaches the Circuits Laboratory course. He is a graduate of the American Meteorological Society's (AMS) Early Career Leadership Academy (ECLA) and the recipient of the 2019 American Meteorological Society's Spiros G. Geotis Student Prize, for his article titled Design of Practical Pulse Compression Waveforms for Polarimetric Phased Array Radar.

Sebastián M. Torres (Senior Member, IEEE) received the B.S. degree from the National University of Mar del Plata, Mar del Plata, Argentina, in 1995, and the M.S. and Ph.D. degrees in electrical engineering from The University of Oklahoma, Norman, OK, USA, in 1997 and 2001, respectively.

In 1997, he joined the Cooperative Institute for Mesoscale Meteorological Studies, The University of Oklahoma, where he is the Assistant Director and a Senior Research Scientist with the National Severe Storms Laboratory (NSSL). He is also the Leader of the Advanced Radar Techniques Group, NSSL, where he is conducting research and development of innovative signal processing and adaptive sensing techniques to improve the quality, coverage, accuracy, and timeliness of meteorological products from weather radars. He is involved in the exploration and demonstration of unique capabilities offered by phased-array radar for weather observations, and the transfer of technology to existing radar systems in government, public, and private organizations.

Dr. Torres has received the 2011 Department of Commence Gold Medal as a member of the Radar Research and Development Division at NSSL for scientific and engineering excellence in adapting military phased-array-radar technology to improve U.S. weather radar capabilities, and the 2003–2004 Office of Oceanic and Atmospheric Research Outstanding Scientific Paper Award. He holds Adjunct Faculty position with the School of Electrical and Computer Engineering, and is a member of the Graduate Faculty and the Advanced Radar Research Center at The University of Oklahoma.

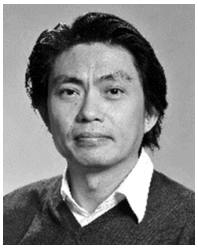

Tian-You Yu (Member, IEEE) received the Ph.D. degree in electrical engineering from the University of Nebraska–Lincoln, Lincoln, NE, USA, in 2000.

In 2002, he joined The University of Oklahoma (OU), Norman, OK, USA. He is the Presidential Professor with the School of Electrical and Computer Engineering and an Adjunct Professor with the School of Meteorology, OU. He also serves as the Directors for the Operations at the Advanced Radar Research Center (ARRC), which is an Interdisciplinary Research Center. He then worked with the National Center for Atmospheric Research (NCAR) as a Post-Doctoral Fellow. This experience has provided him a unique cross-disciplinary background of atmospheric research using various sensors. His expertise includes the development and design of novel and sophisticated radar techniques with the goals of improving radar measurement, enhancing the warning of severe and hazardous weather, and advancing the fundamental knowledge of meteorological phenomena. In parallel with his technical strength, he has a passion for delivering high-quality education. He has developed and taught several undergraduate and graduate courses in the field of radar technology and science at OU.